Fermi National Accelerator Laboratory

FERMILAB-Conf-93/088

Charmonium Physics from $\bar{p}p$ Interactions

R. Ray

Fermi National Accelerator Laboratory
P.O. Box 500, Batavia, Illinois 60510

April 1993

Presented at the *5th Annual Hadron Spectroscopy Summer School,*
University of Maryland, August 17-21, 1992

Disclaimer

Charmonium Physics from $\bar{p}p$ Interactions

R. Ray
Fermi National Accelerator Laboratory

From lectures presented at the 5^{th} annual Hadron Spectroscopy Summer School,
University of Maryland, August 17 - 21, 1992.

Contents

1 Introduction

Heavy quarkonium is perhaps the best QCD laboratory in existence. Much of what we presently know about the fundamental interactions in nature has resulted from the study of two-body bound states. The hydrogen atom, the deuteron and positronium have provided valuable mechanisms for studying quantum mechanics, the theory of nuclear forces and QED. In the same way, one might hope that the study of two-body bound state systems built from heavy quarks will lead to a detailed understanding of at least some of the fundamental properties of strong interactions.

While it is possible to gain some qualitative insights into strong interactions by studying bound states built from light quarks, it is not possible to reach more precise conclusions because of the additional complexities introduced by large relativistic corrections and long range confinement. Charmonium, $c\bar{c}$ bound states, has provided us with the first QCD laboratory where the system could be considered to be at least approximately non-relativistic while at the same time lending itself to perturbative calculations. The substantial mass of the charmed quark ($m_c \sim 1.5$ GeV) corresponds to bound states sufficiently small to begin to probe the asymptotically free component of the strong interaction. The study of $c\bar{c}$ as well as $b\bar{b}$ bound states has greatly enhanced our understanding of the strong interaction between elementary particles. The scope of this article will be to review what has been learned to date, particularly on the experimental front, as well as to look at what remains to be done.

2 Discovery of the c quark

Prior to 1974, two lepton doublets (e and μ) and three quark flavors (u,d,s) were known to exist. The original motivation for a fourth quark was primarily an aesthetic one intended to lend symmetry to the quark and lepton sectors [1]. More convincing technical arguments were put forth in 1970, showing that the introduction of a fourth quark could eliminate the problem of unwanted strangeness-changing neutral currents and could alleviate other higher order problems.

In the case of the leptons, coupling to the W takes place only within a particular SU(2) doublet, giving rise to conservation of electron and muon numbers. The coupling of the W to quark doublets is not quite so simple however. Decays such as $\Lambda \rightarrow p + e + \overline{\nu_e}$ involve the coupling $s \rightarrow u + W^-$ across generational boundries. In 1963, when only the u, d and s quarks were known to exist, Cabibbo [2] suggested that the W coupled, not to the physical quarks, but to the Cabibbo rotated states u and d_c where

$$d_c = d cos\theta_c + s sin\theta_c. \tag{1}$$

θ_c is known as the Cabibbo angle. This prescription gives strangeness-conserving processes a strength $cos\theta_c$ while strangeness-changing processes in which the d quark is replaced by an s quark have a strength $sin\theta_c$. Experimentally, it has been determined that $sin\theta_c \sim 1/5$, thus the strangeness-changing processes are 20 times weaker than strangeness-conserving processes. The weak interactions are therefore seen to *almost* respect quark generations.

Cabibbo's theory was very successful in predicting any number of weak decay rates, but it could not account for the extremely small rate of decay measured for the process $K_L \rightarrow \mu^+\mu^-$. This was just one symptom of a very general problem related to the observed suppression, relative to theoretical expectations, of flavor-changing neutral currents (another related problem was a very large predicted $K_L - K_S$ mass difference). The diagram for this process is shown in figure 1. Although this diagram would seem to contribute to the second-order weak interaction, the loop integral enhances its strength, making it comparable to a first-order diagram.

This problem prompted Glashow, Iliopoulos and Maiani to propose a radical new solution which has come to be known as the GIM mechanism [3]. The GIM mechanism predicts the existence of a fourth quark, the charmed or c quark, in an SU(2) doublet with s_c where

$$s_c = s\cos\theta_c - d\sin\theta_c. \tag{2}$$

The new quark is given a new quantum number, charm (C), which is conserved in strong and electromagnetic interactions in the same way as strangeness (S). The c quark now couples through the charged current to s_c, re-establishing symmetry between the two quark doublets and the two lepton doublets. Suppression of the decay rate of $K_L \rightarrow \mu^+\mu^-$ is re-established by the addition of the diagram in figure 2, where the amplitude is proportional to -$\cos\theta_c\sin\theta_c$, which cancels the diagram in figure 1, where the amplitude is proportional to $\cos\theta_c\sin\theta_c$. The cancellation is, in fact, not exact due to the mass difference between the u and c quarks leaving a small, but finite branching ratio for $K_L \rightarrow \mu^+\mu^-$. Additionally, by introducing only diagonal terms in the neutral current (u-u, d-d, s-s and c-c couplings only) diagrams such as the one in figure 3 are forbidden, thus effectively eliminating strangeness-changing interactions.

In spite of the technical success of the GIM theory, it was not taken very seriously at first. Proposing the existence of a new quark to fix a few esoteric theoretical problems seemed a bit extreme to many. That all changed in November of 1974 when the physics world was shaken by the discovery of a new and very odd particle, the $J/\psi(3097)$. The J/ψ was independently discovered by two groups almost simultaneously. One group [4], working at Brookhaven National Laboratory, saw it as an enhancement in the reaction

$$pBe \rightarrow e^+e^- + anything \tag{3}$$

while another group [5], working at the SPEAR machine at SLAC, saw it in the reaction

$$e^+e^- \rightarrow hadrons. \tag{4}$$

The data was soon independently confirmed by another group at Frascati [6] who also observed reaction 4. A few days after the discovery of the J/ψ another heavier state was found with a mass of 3684 MeV at SPEAR. It was interpreted as being the ψ', the first radial excitation of the J/ψ. Analysis of the shapes of the yield curves, taking into account the broadening due to finite beam-energy spread and initial-state radiation, led to determination of the full widths 69 $\pm$ 15 keV and 228 $\pm$ 56 keV for the J/ψ and ψ', respectively.

These new particles, and the others which would soon follow, were taken to be bound state mesons of the form $c\bar{c}$, built from the charmed quarks first hypothesized 10 years previous. The properties of these particles demonstrate quite conclusively that this is the case.

It was quite remarkable to have found a new particle with such a large mass and yet such a narrow width. Ordinary strong interaction resonances have widths which are typically on the order of a few hundred MeV and seem to increase with increasing resonance mass. While the J/ψ total width is so stunningly small, its leptonic width into e^+e^- is about 4.8 $\pm$ 0.6 keV which is typical of ordinary vector mesons.

The OZI rule was invented to describe the decay of the ϕ meson, but it can also be invoked to help understand the the width of the J/ψ. The OZI rule was formulated independently by Okubo, Zweig and Iizuka [7] and postulates that disconnected quark diagrams are suppressed relative to connected diagrams. The ϕ is a bound $s\bar{s}$ state, permitting the OZI allowed and forbidden decay diagrams of figure 4a and 4b to K^+K^- and 3π, respectively. From the diagrams, one would imply that the decay rate of $\phi \rightarrow 3\pi$ is suppressed relative to the decay rate of $\phi \rightarrow K^+K^-$. The fact that the width of the ϕ is about 4 MeV, a factor of 20 or so smaller than a typical hadronic decay width, is due to the fact that the OZI allowed decay has very little phase space available to it since the ϕ mass is just barely above the $K\overline{K}$ threshold.

In direct analogy with the ϕ meson, one would expect the J/ψ to decay predominantly into pairs of charmed and anti-charmed mesons. However, the lightest charmed meson, the D^0, has a mass of 1863 MeV leaving the $J/\psi(3097)$ (as well as the ψ') below the $D\overline{D}$ mass threshold. As a result, the J/ψ must decay to particles which do not contain charmed quarks. So the narrowness of the J/ψ is the result of energy conservation which only allows decay through OZI suppressed channels.

The OZI rule has never been placed on a firm dynamical foundation and it should be considered only as a phenomenological selection rule. The same principles can be better described in terms of the QCD rules for the coupling of quarks and gluons.

The discovery of these new particles, which brought the 1976 Nobel Prize to Ting and Richter, initiated a string of experimental discoveries. The experimental status of charmonium spectroscopy is shown in figure 5. There would seem to be a large number of radial excitations of the J/ψ (some of these may actually be mixtures of various states) in direct analogy to the case of positronium. The states lying above the $D\overline{D}$ threshold are fairly broad resonances while those lying below the open charm threshold are relatively narrow, as dictated by the OZI mechanism.

The existence of charmed mesons, a bound state containing a c quark and one of the light antiquarks, was predicted in the original paper of Bjorken and Glashow [1]. The charmed D meson was discovered at SLAC in 1976 through production in e^+e^- annihilation [8]. Since the charm quantum number is conserved in strong and electromagnetic interactions, the D meson can only decay through weak interactions. Since weak interactions do not conserve parity, one should expect to observe parity non-conservation in the decay of the D meson. Parity violation was indeed observed in the Decay of the D meson at SLAC by studying the Dalitz plot of the decays $D^+ \rightarrow K^-\pi^+\pi^+ +$ C. C. [9].

Excitations of the D mesons, known as the D^* mesons, have also been observed.

The D^* mesons decay strongly into $D\pi$ and electromagnetically into $D\gamma$.

When all of this information is taken together; the narrow peaks below $D\overline{D}$ threshold, the broad peaks above threshold, intermediate P states, D mesons with parity non-conserving decays, and excited D^* mesons, there can be little doubt as to the existence of the predicted c quark.

3 Basics of QCD

Quantum chromodynamics (QCD) is the only serious candidate for the theory of strong interactions. The term chromodynamics was coined by Gell-Mann in reference to the most fundamental property of quarks; their color. Color was first introduced to resolve a problem with the Fermi statistics of the Ω^- hyperon, a spin 3/2 object built from three identical fermions (s quarks) with their spins aligned. A new quantum number was needed to differentiate the quarks from one another and to restore the Pauli principle. This new degree of freedom was color.

All of the fundamental interactions are thought to respect symmetry under color exchange. This symmetry can be viewed as a new SU(3) symmetry which we will refer to as $SU(3)_c$, not to be confused with the ordinary SU(3) of flavor. Unlike ordinary SU(3), $SU(3)_c$ is an exact symmetry. This leads to the requirement that all ordinary hadrons which appear as free particles must must be color singlets, meaning they have no net color.

QCD is constructed by extending the global $SU(3)_c$ symmetry to a local gauge symmetry. This leads to the introduction of 8 massless vector gauge fields, or colored gluons, which interact with the spin 1/2 quark fields which come in 3 colors. The gluons mediate the force between quarks and couple to color in much the same way as photons mediate the electromagnetic force by coupling to charge. Since gluons carry color, they not only interact with quarks, but with each other, resulting in an inherently nonlinear theory. Such theories are referred to as non-Abelian.

While QCD bears some similarity to QED, QCD is actually a much more complicated theory. QCD is a renormalizable theory, like QED, so that the ultraviolet divergencies that normally appear in perturbation theory can be handled in the usual way. QCD is known to possess the rather amazing property of asymptotic freedom and is thought to possess the property of color confinement. These two properties, for which there is no QED analog, are the most important characteristics of QCD for the purposes of our discussion.

In QED, the loop diagram in figure 6, where a virtual photon momentarily converts into an e^+e^- pair, leads to a dependence of the electromagnetic coupling constant α on the momentum transfer q:

$$\alpha(|q^2|) = \alpha(0)[1 + \frac{\alpha(0)}{3\pi} ln(|q^2|/(mc)^2] \quad (|q^2| = -q^2 \gg (mc)^2). \tag{5}$$

Equation 5 is only valid to order $\alpha(0)^2$. As the distance between charges is decreased, corresponding to larger $|q^2|$, the electromagnetic coupling strength increases as 1/r. This is interpreted as a consequence of 'vacuum polarization' where the vacuum possesses dialectric properties which leads to partial screening of the charge. The charges

experience less screening as they are brought closer together, thus increasing the effective charge.

We see a similar process in QCD where the diagram in figure 7, in which a gluon couples momentarily to a $q\bar{q}$ pair, gives rise to color screening of much the same form as that expressed in equation 5. Additional complications arise in QCD because of the self interaction of gluons which give rise to diagrams such as that in figure 8. The contribution from the gluon loop diagrams act in the opposite direction from the contribution due to the $q\bar{q}$ loop in figure 7, resulting in 'antiscreening'. The QCD running coupling constant, when all of these factors are included, is:

$$\alpha_s(|q^2|) = \frac{\alpha_s(\mu^2)}{1 + (\alpha_s(\mu^2)/12\pi)(11n - 2f)ln(|q^2|/\mu^2)} \qquad (|q^2| \gg \mu^2) \qquad (6)$$

where n is the number of colors (3) and f is the number of flavors (6). We see that if 11n>2f, antiscreening will dominate over screening and the coupling constant will decrease as the particles are brought closer together (larger $|q^2|$). This effect is the well known 'asymptotic freedom', which tells us that the strong force becomes weaker at small distances.

In QED, we define $\alpha(0)$ as the old fine structure constant, equal in value to 1/137. This was chosen as a matter of convenience and because it is small enough to be a sensible parameter for perturbative expansions. However, α_s defined at q^2=0 is quite large and not at all appropriate for perturbative expansions. That is why we choose our reference value as $\alpha_s(\mu^2)$. The value that we choose for μ is unimportant so long as $\alpha_s(\mu^2) < 1$.

As strongly interacting particles are pulled apart, the coupling constant becomes quite large. This is presumably one basis for quark confinement, which says that isolated quarks cannot appear in nature and that all physical hadrons are color singlets. The presumption is that the potential energy between two quarks increases without bound as they are pulled apart until the energy invested is large enough to create new quark-antiquark pairs. While this notion is generally accepted, it has never actually be proven that QCD leads naturally to confinement. The difficulty lies precisely in the fact that the magnitude of the strong coupling constant at large distances, which leads to confinement, also makes perturbative calculations, and hence Feynman calculus, impossible.

4 Potential Models

One of the most satisfying aspects of heavy $q\bar{q}$ spectroscopy is the ability of QCD inspired phenomenological models to describe the general features of particle spectra. The predictive power is due, in large part, to the heavy mass of the quarks which allows the use of non-relativistic dynamics (the Schrödinger equation) in much the same way as can be applied to the hydrogen atom and positronium. In the case of the hydrogen atom and positronium we know precisely what potential to plug into the Schrödinger equation. That is no longer true as we move into the realm of strong

interactions. Even though we don't know the precise form of the hadronic potential, we can use what we know about QCD to make a reasonable guess.

The overall details of the experimental picture have been adequately described in terms of QCD inspired potential models which incorporate the ideas of QCD into the familiar language of scattering theory. Such models generally assume:

1. Non-relativistic dynamics apply to lowest order and relativistic corrections are small;

2. one-gluon exchange dominates at small distances;

3. multiple gluon exchange dominates at large distances and leads to confinement.

Because the strong coupling constant is relatively weak at short distances (asymptotic freedom), the probability of coupling to multiple gluons is small and the $c\bar{c}$ interaction is dominated by single gluon exchange. Recall that quarks carry color, so the exchange of a single colored gluon between two colored quarks is permitted. Single gluon exchange at short distance is similar to the exchange of a single photon between charged objects and results in a Coulomb-like potential of the type

$$V(r) = -\frac{4}{3}\frac{\alpha_s(r)}{r} \tag{7}$$

where the factor of 4/3 arises from the $SU(3)_c$ algebra.

At large distances, on the order of 1 fm or larger, the strong coupling constant grows in strength and the probability of multiple-gluon coupling becomes large compared to single gluon coupling ($\alpha_s > 1$). Phenomenologically, this can be thought of as a bunching together of the lines of force into a tube of constant cross-sectional area. By Gauss' Law, this leads to a linear potential of the form

$$V(r) = kr \tag{8}$$

where k is a proportionality constant. This spring-like potential confines the quarks such that they may never separate from one another and appear as separate entities.

Light quark mesons are intrinsically relativistic due to the fact that the binding energies are not small when compared to the constituent masses. When evaluating the hydrogen atom and positronium, nonrelativistic quantum mechanics is used and a relativistic correction term is added. Since we cannot exactly solve the relativistic bound state problem, we must hope that heavy quarkonium states can be treated in the same way, as more or less nonrelativistic systems.

It would be appropriate at this time to investigate the degree to which charmonium is non-relativistic. We choose to evaluate this through the use of the virial theorem

$$2 < T > = < \vec{r} \cdot \vec{\nabla} V(\vec{r}) > \tag{9}$$

where T is the kinetic energy of the system and <> indicates an expectation value. Assume a linear potential, as in equation 8. Then

$$2 < T > = < V > \tag{10}$$

and, from the non-relativistic expression for kinetic energy of two quarks $< T >= 2(m_Q/2) < v^2 >$ and the energy relation $E =< T > + < V >$ we obtain

$$< v^2 >= E/3m_Q. \tag{11}$$

The binding energy of charmonium can be estimated as

$$E \sim M_{D\overline{D}} - M_\psi = 638MeV. \tag{12}$$

For a charmed quark effective mass of 1.5 GeV this leads to

$$< v^2 > \sim 0.14. \tag{13}$$

Similarly for bottomonium, $E \sim 1096$ MeV, $m_b \sim 5$ GeV and

$$< v^2 > \sim 0.07. \tag{14}$$

To evaluate a similar expression for the light quarks we will assume that the binding energy is defined by the $\rho - \pi$ mass splitting and that the effective mass of a light quark is about 300 MeV. From this we arrive at

$$< v^2 > \sim 0.7 \tag{15}$$

for the light quarks. So we see that while charmonium is more or less non-relativistic, the non-relativistic assumption works much better for bottomonium. As expected, the assumption breaks down entirely in the light quark sector. Other potentials give similar results. This treatment should perhaps not be taken too literally, since we have used non-relativistic expressions to determine the degree to which a system is non-relativistic. Nevertheless, the results give one an appreciation for the relative magnitude of the situation.

4.1 Spin Dependence

Most of the interesting aspects of the charmonium spectrum are the result of spin dependence. When spin is incorporated into the potential models spin-orbit interactions (fine structure), spin-spin interactions (hyperfine structure) and tensor interactions result. At the same time, one must give up on a purely non-relativistic treatment in order to include spin.

The precise character of the spin-dependent parts of the potential will depend on the Lorentz structure of the interaction. The short-range part of the interaction corresponds primarily to one-gluon exchange and should therefore be vector in nature, in direct correlation to the case of positronium. The long-range part of the potential is due to the exchange of multiple gluons and has no direct analogy to positronium. The long-range part of the potential can therefore contain scalar and vector terms as well as anomalous moment terms. The problem is that we don't know how much of the potential is scalar and how much is vector.

The spin-orbit interaction, which includes the Thomas precession term, is generally thought to be a long range interaction while the spin-spin and tensor interactions are thought to be short range interactions.

The spin-orbit interaction between quarks results from both the scalar ($V_s(r)$) and vector ($V_v(r)$) parts of the potential and has the form

$$E_{so} = \frac{(3\frac{dV_v}{dr} - \frac{dV_s}{dr})}{2m^2 r}(\vec{L}\cdot\vec{S}) \tag{16}$$

The contribution from $V_v(r)$ arises from both the explicit spin-orbit interaction and Thomas precession, while the contribution from V_s is due only to Thomas precession.

The vector part of the potential also gives rise to a tensor interaction, which may be written as

$$E_T = \frac{S_{12}}{12m_1m_2}\left(\frac{1}{r}\frac{dV_v}{dr} - \frac{d^2V_v}{dr^2}\right) \tag{17}$$

where $S_{12} = 2[3(\vec{S}\cdot\hat{r})(\vec{S}\cdot\hat{r}) - S^2]$ is non-zero only for states with L$\neq$0.

The hyperfine spin-spin interaction due to single gluon exchange is responsible for the splittings of the π and the ρ mesons and the nucleon and the Δ resonance in the light quark sector. The spin-spin interaction for two quarks of identical mass is of the form

$$E_{ss} = \frac{\vec{\sigma_1}\cdot\vec{\sigma_2}}{6m^2}\bigtriangledown^2 V_v(r) \tag{18}$$

where σ_1 and σ_2 are the Pauli matrices which describe the spin of the quark and antiquark. The expectation value of $\vec{\sigma_1}\cdot\vec{\sigma_2}$ = -3 when S=0 (singlet state) and 1 when S=1 (triplet). Only the short range vector part of the potential contributes to the spin-spin interaction. If we assume that the vector part of the interaction is described by equation 7 then

$$E_{ss} = \frac{8\pi\alpha_s\vec{\sigma_1}\cdot\vec{\sigma_2}}{9m^2}\delta^3(\vec{r}). \tag{19}$$

The δ function forces all expectation values to zero other than those between S states. Verifying the absence of appreciable spin-spin splitting for states with L>0 is therefore an interesting probe of the short range part of the potential.

5 Decays of Charmonium states

Perturbative QCD expressions and first order corrections for annihilation decay rates have been calculated by Kwong, Rosner and Quigg [47]. This is an ideal reference and should be consulted for details.

Decays through one virtual photon of the type

$$Q\bar{Q} \rightarrow \gamma^* \rightarrow l^+l^- \tag{20}$$

are relevant for $Q\bar{Q}$ states with the same quantum numbers as the photon; $J^{PC} = 1^{--}$. These correspond to the n^3S_1 states such as the J/ψ and ψ'.

Two photon decays are possible for both S-wave and P-wave states. Recall that C=(-1)$^{L+S}$ and that C($\gamma\gamma$) =(-1)(-1) = +1. This implies that only spin-0 S-wave states and spin-1 P-wave states can decay to $\gamma\gamma$. These include the η_c and η_c' resonances (n$^1S_0$) and the χ_0 and χ_2 ($^3P_{0,2}$). The $^3P_1$ decay to $\gamma\gamma$ is forbidden by Yang's theorem [11].

Three photon decays of n$^3S_1$ states are also allowed, though they are somewhat rare due to the α^3 dependence of the annihilation rate.

According to the laws of QCD, the decay of a charmonium state into hadrons is the result of the annihilation of the c and $\bar{c}$ quarks into gluons. The number of gluons is determined by the various conservation laws. Because the large mass of the charmed quark dictates that annihilation takes place at small distances where the strong coupling constant is small, we will always concern ourselves only with the minimal number of gluons. The selection rules for $c\bar{c}$ annihilation are very similar to the rules for positronium annihilation.

The C parity for any fermion-antifermion system is given by $C = (-1)^{L+S}$, while the C parity for gluons is a bit more complicated and the reader is referred to reference [10] for details.

The exact SU(3)$_c$ symmetry of QCD forbids annihilation to a single gluon, since gluons carry color while the physical hadrons to which they must couple are color singlets. For two-gluon decays, the selection rules are identical with those of positronium. Two-gluon decays are allowed for all C-even states with total spin J$\neq$ 1. The annihilation rate to gg is proportional to α_s^2.

A massive spin-1 object may not decay to two identical massless spin-1 objects according to Yang's theorem [11]. Thus, two-gluon decays of J=1 charmonium states are forbidden. However, if one of the gluons is virtual and materializes into a $q\bar{q}$ pair, the symmetry upon which Yang's theorem is built vanishes and the process is allowed. This is the process which determines the width of the $^3P_1$ (χ_1) state of charmonium, for example. The annihilation rate for such decays goes as α_s^3.

Table 1: Gluon coupling configuration of various $q\bar{q}$ states

$q\bar{q}$ state	$^1S_0$	$^3S_1$	$^1P_1$	$^3P_0$	$^3P_1$	$^3P_2$
J^{PC}	0^{-+}	1^{--}	1^{+-}	0^{++}	1^{++}	2^{++}
gluon coupling	2g	3g	3g	2g	3g	2g
					$gq\bar{q}$	

Any quark-antiquark state can couple to three-gluons. There are two independent ways in which one may combine three members of a color octet in order to obtain a color singlet. One of these combinations turns out to be C-even while the other is C-odd. This is contrary to the case of positronium where three photons may couple only to C-odd states. The annihilation rate to three gluons is proportional to α_s^3.

The minimal gluon coupling configuration for the various quark-antiquark states is listed in table 1. An understanding of just these simple selection rules leads to a

number of general insights into the total widths and branching ratios of charmonium states.

5.1 Dipole Transition Rates

Dipole transitions are particularly interesting because they can be understood to a large degree using simple quantum mechanics, though they are quite susceptible to relativistic effects.

The rate of electric dipole, or E1, transitions of the type $\Gamma(n^3S_1 \rightarrow n'^3P_J\gamma)$ and $\Gamma(n^3P_J \rightarrow n'^3S_1\gamma)$ is

$$\frac{4\alpha e_Q^2 E_\gamma^3}{27}(2J_f+1)|<f|r|i>|^2 \tag{21}$$

where i and f are the normalized radial wavefunctions of the initial and final states, J_f is the spin of the final state and e_Q is the quark charge (2/3 for c) in units of e. Similarly, the rate of magnetic dipole, or M1 transitions of the type $\Gamma(n^3S_1 \rightarrow n'^1S_0\gamma)$ and $\Gamma(nS_0 \rightarrow n'^3S_1\gamma)$ is

$$\frac{4\alpha e_Q^2 E_\gamma (2J_f+1)}{3M_Q^2}|<f|j_0(E_\gamma r/2)|i>|^2 \tag{22}$$

where j_0 is a spherical Bessel function. In the long wavelength limit, the expectation value $|<f|j_0(E_\gamma r/2)|i>|$ reduces to 0 or 1, depending on the quantum numbers of the initial state. Because of the orthogonality and normalization properties of the radial wavefunction R(r), we have:

$$\int r^2 R_i(r)R_f(r)dr = 1 \quad n=n' \qquad \int r^2 R_i(r)R_f(r)dr = 0 \quad n\neq n'. \tag{23}$$

We refer to the case where $n = n'$ as 'allowed M1 transitions' and the case where $n \neq n'$ as 'hindered M1 transitions.' Corrections to 23 are known to be as large as 50%. Observation of the hindered M1 transition $\psi' \rightarrow \eta_c\gamma$ indicates that relativistic corrections are not insignificant in the charmonium system. The corresponding decay in the $b\bar{b}$ system has not yet been seen as the η_b has yet to be discovered.

Each multipole has a definite parity and is subject to angular momentum conservation. l_γ is the total angular momentum carried off by the emitted γ-ray:

$$|J_i - J_f| \leq l_\gamma \leq J_i + J_f. \tag{24}$$

Since $R << \lambda$ and since the transition probabilities associated with higher multipoles become smaller by increasing powers of $(R/\lambda)^2$, the lowest multipole allowed by the selection rules is expected to dominate. The selection rules are:

$$\begin{aligned} P_i \cdot P_f &= (-1)^L \qquad \text{E(L) pole} \\ P_i \cdot P_f &= -(-1)^L \qquad \text{M(L) pole} \\ L &> 0 \qquad \text{no monopole radiation.} \end{aligned}$$

Additionally, transitions between states with the same C quantum number are prohibited since a γ-ray is a C=-1 state.

Consider, for example the decay ${}^3P_2 \rightarrow {}^3S_1\gamma$. The ${}^3P_2$ is a $J^{PC} = 2^{++}$ state while the ${}^3S_1$ is a 1^{--}. Thus:

$$P_i \cdot P_f = -1 \qquad \Delta J = 1 \Rightarrow \qquad l_\gamma = 1, 2, 3$$

$$\begin{aligned} l = 1 \Rightarrow \quad & P_i \cdot P_f = (-1)^1 = -1 \quad E1 \\ l = 2 \Rightarrow \quad & P_i \cdot P_f = -(-1)^2 = -1 \quad M2 \\ l = 3 \Rightarrow \quad & P_i \cdot P_f = (-1)^3 = -1 \quad E3 \end{aligned}$$

The lowest allowed multipoles for allowed radiative transitions are shown in table 2.

Table 2: The lowest allowed multipoles for radiative transitions

	$P_i \cdot P_f$	$C_i \cdot C_f$	lowest allowed multipole
${}^3S_1 \leftrightarrow {}^3P_{0,1,2}$	-1	-1	E1
${}^1S_0 \leftrightarrow {}^1P_1$	-1	-1	E1
${}^3S_1 \leftrightarrow {}^1S_0$	+1	-1	M1
${}^3P_{0,1,2} \leftrightarrow {}^1P_1$	+1	-1	M1

The hypothesis that only one quark in a $Q\bar{Q}$ meson is involved in radiating a photon in a radiative transition, known as the Single Quark Radiation (SQR) hypothesis [48], has implications for the number of allowed multipole transitions. Consider ${}^3P_2 \rightarrow {}^3S_1$. If we now let J_i and J_f correspond to the total angular momentum of one quark orbiting about a spectator quark then, recalling that the total orbital angular momentum of the system is 1, we have:

$$\begin{aligned} J_i + 1/2 = 2 \Rightarrow \qquad & J_i = 3/2 \\ J_f + 1/2 = 1 \Rightarrow \qquad & J_f = 1/2 \end{aligned}$$

$$l_\gamma = 1, 2 \Rightarrow \qquad \text{no E3 transition allowed.}$$

Testing the SQR hypothesis then reduces to measuring the contributions of the various multipoles to particular radiative transitions.

6 Brief Survey of Charmonium States

The J/ψ and ψ' have been well studied and documented elsewhere, so they will not receive any treatment here.

6.1 The ^3P states

Next to the J/ψ and ψ', the ^3P_J or $\chi_{0,1,2}$ states are the most thoroughly studied. The χ states all have J^{PC} quantum numbers of J^{++}. The most relevant parameters of the χ states, prior to the recent work of E760 at Fermilab, are listed in table 3. The χ states were originally discovered in radiative decays of the ψ'. The χ_1 decays predominantly through $q\bar{q}g$ while the χ_0 and χ_2 decay through gg. $\Gamma(\chi_0) > \Gamma(\chi_2) > \Gamma(\chi_1)$ and the ratio of the widths of the χ_2 and χ_0 is predicted from theory to first order to be

$$\frac{\Gamma(\chi_2 \to gg)}{\Gamma(\chi_0 \to gg)} = 4/15. \tag{25}$$

Recently, a fair amount of precision work has been done on the χ_1 and χ_2 states. This will be described later.

Table 3: Parameters of the χ states prior to E760

	χ_0	χ_1	χ_2
Mass(MeV)	3415.1 ± 1.0	3510.6 ± 0.5	3556.3 ± 0.4
Total Width (MeV)	13.5 ± 5.3	< 1.3 (95% CL)	$2.6\ ^{+2.6}_{-0.9}$
$BR(\chi \to J/\psi\gamma)$	$(6.6 \pm 1.8) \times 10^{-3}$	$(27.3 \pm 1.6)\%$	$(13.5 \pm 1.1)\%$

6.2 The $^1S_0$ States

The singlet states of heavy quarkonia (S=0, J=L, P=$(-1)^{(L+1)}$, C=$(-1)^L$) pose an unusual experimental challenge because they can be neither resonantly produced in e^+e^- annihilation into a virtual photon (J^{PC}=1^{--}) nor populated by E1 decay of the $^3S_1$ states. To date only the η_c (1^1S_0, 0^{-+}) has been positively identified [17]. An early claim for the η_c' (2^1S_0, 0^{-+}) [29] remains unconfirmed, and searches by the Crystal Ball collaboration and R704 failed to find the $h_c(1^1P_1$ (1^{+-})) state of Charmonium [24, 30].

The η_c was discovered in M1 transitions from both the J/ψ and the ψ'. It has also been seen in $p\bar{p}$ interactions and in $\gamma\gamma$ interactions of the type indicated in figure 9 [50]. The mass of the η_c has been measured to be 2979.6 ± 1.6 MeV and its total width measured to be $10.3\ ^{+3.8}_{-3.4}$ MeV [17]. The decay $\eta_c \to \gamma\gamma$ has been measured, though not terribly well as the errors on the branching ratio $BR(\eta_c \to \gamma\gamma) = (6^{+6}_{-5}) \times 10^{-4}$ would indicate.

The η_c' has only been seen by the Crystal Ball experiment. The signal is not overwhelming and has never been confirmed by another group. The Crystal Ball obtained a mass of 3592 ± 5 MeV and a 95% CL of less than 8 MeV for the total width of the η_c'. From Kwong, Rosner and Quigg [47]:

$$\frac{\Gamma(\eta_c')}{\Gamma(\eta_c)} \sim \frac{\Gamma(\eta_c' \to gg)}{\Gamma(\eta_c \to gg)} = \frac{|\psi(0)|'^2}{|\psi(0)|^2} \tag{26}$$

where $\frac{|\psi(0)|'^2}{|\psi(0)|^2}$ is obtained from the leptonic widths of the ^3S states:

$$\frac{\Gamma(\psi' \to e^+e^-)}{\Gamma(\psi \to e^+e^-)} = \frac{|\psi(0)|'^2}{|\psi(0)|^2}\frac{M_\psi^2}{M_{\psi'}^2}. \tag{27}$$

Plugging in the appropriate numbers results in $\frac{\Gamma(\eta_c')}{\Gamma(\eta_c)} \sim 0.64$ and $\Gamma(\eta_c') \sim 6$ MeV.

The mass of the η_c' is predicted to be somewhere in the range between 3540 - 3630 MeV. A recent calculation [49] of the partial width of $\eta_c' \to \gamma\gamma$ gives a result of 3.5 keV and $\mathrm{BR}(\eta_c' \to \gamma\gamma) = 5.8 \times 10^{-4}$.

6.3 The $^1P_1$ State

As previously mentioned, the $^1P_1$ state is another example of a singlet state which is very difficult to produce and to study. The $^1P_1$ state of charmonium ($J^{PC} = 1^{+-}$) had never been seen until the recent observation by E760 at Fermilab. The Crystal Ball and R704 both searched unsuccessfully for the $^1P_1$. The E760 data for the $^1P_1$ state will be discussed in detail later.

The mass of the $^1P_1$ is a subject of considerable interest as it provides an interesting test of our understanding of spin-dependence in $c\bar{c}$ interactions. In the limit that all of the spin-dependant terms are sufficiently small to be treated perturbatively, only the spin-spin term E_{ss} contributes to the spin-weighted center-of-gravity of the ^3P states and to the deviation of the $^1P_1$ mass from the center-of-gravity:

$$m_{c.o.g.} = \frac{m_{\chi_0} + 3m_{\chi_1} + 5m_{\chi_2}}{9} = < M(P) > + < E_{ss} > \tag{28}$$

and $\mathrm{M}(^1P_1) = < M(P) > -3 < E_{ss} >$[19], where the brackets denote expectation values. In this simple framework, the mass of the $^1P_1$ will probe the degree to which spin-spin forces are truly negligible for states with L>0.

A more sophisticated and quite recent calculation of the $^1P_1$ mass [20] from gluon exchange finds that the one-loop QCD correction is independent of both renormalization scale and renormalization scheme and that the splitting depends only on $\alpha_s(m_c)$ and the radial wave function. The authors conclude that the $^1P_1$ mass must lie above $m_{c.o.g.}$ and calculate the splitting to be 0.7 ± 0.2 MeV. A number of other predictions may also be found in the literature [32].

The electric dipole (E1) transition $^1P_1 \to \eta_c\gamma$ is expected to be the dominant decay mode of the $^1P_1$ state. However, this decay mode may be sensitive to relativistic corrections which might reduce its rate considerably.

The other likely decay modes of the $^1P_1$ are $J/\psi\pi^0$ and $J/\psi\pi\pi$. The partial widths for these decays are expected to be small since the former does not conserve isospin and the later is suppressed by the limited phase space available and by angular momentum barrier effects.

6.4 The D States

Of the four possible D states ($^1D_2$, $^3D_{1,2,3}$), only the $^3D_1$ has possibly been observed. The $\psi(3770)$ is about 40 MeV above the $D\bar{D}$ threshold and decays primarily to $D\bar{D}$.

The $^3D_1$ shares the same J^{PC} quantum numbers as the $^3S_1$ states allowing for the possibility of mixing. $\Gamma(\psi(3770) \rightarrow e^+e^-) = 0.26 \pm 0.04$ keV which is much larger than one would expect for a pure D state ($\Gamma_{ee} \sim |R''(0)|^2$). Most of the leptonic width of the $\psi(3770)$ is thought to result from an admixture of 2^3S_1.

The $^3D_2$, $^3D_3$ and $^1D_2$ states should all be nearby the $\psi(3770)$. However, $J^P = 2^-$ for both the $^3D_2$ and the $^1D_2$ disallowing decay to two 0^- states ($D\bar{D}$). This follows from the fact that P=$(-1)^l$ for a Boson-anti-Boson pair and that J=2 requires that two spin 0 Bosons be in a relative D wave. From this it follows that P=$(-1)^{l=2} = +1$ which is inconsistent with the $J^P = 2^-$ assignments for $^3D_2$ and $^1D_2$.

$^3D_2$ and $^1D_2$ can, however, decay to $D^*\bar{D}$ as D^* is a 1^- state and can be placed in a relative P wave with $\bar{D}$ to form a J=2 state with $P = (-1)^{l=1} = -1$. $^3D_2$ and $^1D_2$ are predicted to have masses somewhere between the $D\bar{D}(3728)$ and $D^*\bar{D}(3874)$ thresholds [45] disallowing decays to open charm. This holds out the possibility that the $^3D_2$ and $^1D_2$ could be narrow and would decay to lower lying charmonium states. Allowed decays include $^3D_2 \rightarrow J/\psi\pi\pi$, $^3D_2 \rightarrow ^3P_{1,2}\gamma$, and $^1D_2 \rightarrow ^1P_1\gamma$. The first of these decay modes would appear to be the most promising.

7 Formation of $c\bar{c}$ states in $\bar{p}p$ interactions

Most of the experimental work done on charmonium states has been done at e^+e^- machines. e^+e^- interactions are very clean as compared to $\bar{p}p$ collisions where huge hadronic backgrounds pose a formidable challenge to experimenters. In contrast to e^+e^- annihilations where only states with the quantum numbers of the photon ($J^{PC} = 1^{--}$) are directly accessible, one can resonantly produce the full spectrum of charmonium states in $\bar{p}p$ annihilations. States with different quantum numbers must be reached in e^+e^- interactions through transitions from higher mass 1^{--} states. The obvious benefit of resonant formation is that the mass resolution depends only on the accuracy of the particle beam, not the detector resolution. When states are formed through transitions from higher mass states, the resolution of the detector must be relied upon to accurately measure the recoil particles. These recoil particles often carry relatively little energy, making accurate measurement even more difficult. $\bar{p}p$ interactions make precision studies of a number of charmonium states possible for the first time, provided experimenters can learn to deal with the large backgrounds.

The formation cross section for charmonium states is $\leq 10^{-6}$ times that of the hadronic non-resonant background from $\bar{p}p$ interactions. This makes it extreamly difficult to extract a signal when searching for the hadronic decay modes of charmonium states. A much better signal-to-background may be achieved, however, if one focuses on electromagnetic decays of charmonium where the final state contains electrons and gamma-rays. In many cases an almost background free data sample may be obtained, as will be demonstrated shortly.

The charmonium states may be studied by sweeping the $\bar{p}$ energy across the resonances and measuring their cross sections as a function of the center-of-mass energy. The resonance parameters are extracted by an analysis of the resulting excitation curve. The observed excitation curve is the convolution of the Breit-Wigner cross

section for the resonance with the energy distribution function of the beam. The Breit-Wigner cross section for the formation and subsequent decay of a resonance R with total angular momentum J, mass M_R, and total width Γ_R is

$$\sigma_{BW}(E_{cm}) = \frac{(2J+1)}{(2S+1)(2S+1)} \frac{4\pi(\hbar c)^2}{(E_{cm}^2 - 4(m_p c^2)^2)} \frac{\Gamma_R^2 B_{in} B_{out}}{(E_{cm} - M_R c^2)^2 + \Gamma_R^2/4} \ . \quad (29)$$

Here S is the spin of the initial state proton, B_{in} and B_{out} are the branching ratios in the resonance formation channel ($\bar{p}p \rightarrow R$) and in the decay channel respectively. The center-of-mass energy E_{cm} is determined from the $\bar{p}$ beam energy. σ_{peak} is the cross section at $E_{cm} = M_R c^2$, and is given by

$$\sigma_{peak} = (2J+1)[4\pi(\hbar c)^2 B_{in} B_{out}/(E_R^2 - 4(m_p c^2)^2)] \ . \quad (30)$$

If the energy distribution function of the beam is known, then Γ_R can be extracted from an analysis of the shape of the measured excitation function. If $\Gamma_R/\Gamma_B > 1$, where Γ_B is the beam width, then Γ_R may be determined with good accuracy. The precision of the measurement improves as Γ_R/Γ_B increases.

7.1 R704 at the ISR

Experiment R704 at the ISR was the pioneer of this field. By inserting a molecular hydrogen gas jet target into the circulating antiproton beam of the ISR, they were able to form charmonium states from $\bar{p}p$ interactions for the first time. R704 made precision measurements of the χ_1 and χ_2 states of charmonium. R704 also searched, unsuccessfully, for the $^1P_1$ charmonium state. R704 was an unfortunately short-lived experiment, falling victim to the permanent shutdown of the ISR.

I will not focus on R704 here but will describe in detail a more recent second generation experiment, E760 at Fermilab (It should be pointed out that the author is a member of the E760 collaboration). Nevertheless, the mark left on the field by R704 should not be forgotten. The interested reader is referred to R704's published record [12].

8 Experiment 760 at Fermilab

E760 is a charmonium formation experiment performed in the antiproton accumulator ring at Fermilab which was designed for precision studies of reactions of the type

$$p\overline{p} \rightarrow c\bar{c} \rightarrow \text{electromagnetic final states.} \quad (31)$$

The experiment is performed by inserting a molecular hydrogen gas jet target into the machine vacuum of the antiproton ring. This technique was originally pioneered by the R704 collaboration at the ISR. As any good second generation experiment should, E760 enjoys many advantages over its predecessor. E760 has $\sim$ 10 times the instantaneous luminosity, $\sim$ 3 times better beam energy resolution and $\sim$ 5 times larger acceptance than R704. The E760 author list appears on the following page.

The E760 Collaboration

T.A. Armstrong[6], D. Bettoni[2], V. Bharadwaj[1], C. Biino[7], G. Borreani[2], D. Broemmelsiek[4], A. Buzzo[3], R. Calabrese[2], A. Ceccucci[7], R. Cester[7], M. Church[1], P. Dalpiaz[2], P.F. Dalpiaz[2], R. Dibenedetto[7], D. Dimitroyannis[5], M.G. Fabbri[2], J. Fast[4], A. Gianoli[2], C.M. Ginsburg[5], K. Gollwitzer[4], A. Hahn[1], M. Hasan[6], S. Hsueh[1], R. Lewis[6], E. Luppi[2], M. Macrí[3], A.M. Majewska[6], M. Mandelkern[4], F. Marchetto[7], M. Marinelli[3], J. Marques[4], W. Marsh[1], M. Martini[2], M. Masuzawa[5], E. Menichetti[7], A. Migliori[7], R. Mussa[7], M. Pallavicini[3], S. Palestini[7], N. Pastrone[7], C. Patrignani[3], J. Peoples Jr.[1], L. Pesando[7], F. Petrucci[2], M.G. Pia[3], S. Pordes[1], P. Rapidis[1], R. Ray[5,1], J. Reid[6], G. Rinaudo[7], B. Roccuzzo[7], J. Rosen[5], A. Santroni[3], M. Sarmiento[5], M. Savrie[2], A. Scalisi[3], J. Schultz[4], K.K. Seth[5], A. Smith[4], G.A. Smith[6], M. Sozzi[7], S. Trokenheim[5], M.F. Weber[4], S. Werkema[1], Y. Zhang[6], J. Zhao[5], G. Zioulas[4].

[1] *Fermi National Accelerator Laboratory, Batavia, Illinois 60510, U.S.A.*
[2] *I.N.F.N. and University of Ferrara, 44100 Ferrara, Italy*
[3] *I.N.F.N. and University of Genoa, 16146 Genoa, Italy*
[4] *University of California at Irvine, California 92717, U.S.A.*
[5] *Northwestern University, Evanston, Illinois 60208, U.S.A.*
[6] *Pennsylvania State University, University Park, Pennsylvania 16802, U.S.A.*
[7] *I.N.F.N. and University of Turin, 10125 Turin, Italy.*

8.1 The Antiproton Source at Fermilab

The Fermilab Antiproton Accumulator is a storage ring designed to accumulate and cool antiprotons for the Tevatron colliding beam program. The 474 meter ring has been designed to operate at a fixed energy of 8.9 GeV/c^2. In order to provide antiprotons over a range of 4–7 GeV for use in the present experiment, the Accumulator had to be substantially modified.

During the experiment, the Accumulator is run first in its designed mode to accumulate the desired number of antiprotons at 8.9 GeV. Once an adequate number of antiprotons are collected, the beam is decelerated to the desired energy[25]. In a typical run for the present experiment, a beam of up to 3×10^{11} antiprotons is accumulated at an average rate of $\approx 10^{10}\,\bar{p}$/hr.

The internal hydrogen gas jet operates at a typical density of 3.5×10^{13} atoms/cm^2. It has transverse dimensions of ≈ 0.5 cm^2 in the interaction region. The peak luminosity achieved is $\approx 1.0 \times 10^{31}$ cm^{-2}s^{-1}. The luminosity lifetime is 50–100 hours depending on the energy of the beam and the gas jet density, which is occasionally varied. Each store lasts for about 1–2 lifetimes, after which the beam is dumped.

The stochastic cooling[26] system is essential to the success of this experiment. The transverse cooling system counteracts the growth of beam emittance due to the beam's repeated traversal of the gas jet and of the residual gas in the ring. The momentum cooling serves two purposes: it compensates for the average dE/dx loss due to the beam traversing the jet and it narrows the beam energy spread Γ_B to ≈ 0.5 MeV in the center-of-mass.

The average beam energy and the beam energy spread are important for the determination of the mass and width of a narrow resonance. The precision of the beam energy measurement determines the precision of the measurement of the resonance mass. The precision with which the beam energy width is measured directly influences how well the width of a narrow resonance can be determined.

The determination of the average beam energy and the beam energy spread are both based on the measurement of the beam revolution frequency spectrum. The beam energy is determined from the velocity of the beam in the lab frame. The beam velocity is given by:

$$c\beta = fL \ , \tag{32}$$

where f is the revolution frequency of the particles in the beam and L is the orbit length.

The length of the central orbit determined by optical survey is not known with sufficient accuracy to determine the beam energy to the required precision. The orbit length must therefore be calibrated with the known mass of a narrow resonance. The ψ' was chosen. The ± 0.1 MeV/c^2 uncertainty in the published mass of the ψ' corresponds to an uncertainty in the orbit length of ± 0.67 mm at the ψ'.

Having established the reference orbit at the ψ', the center-of-mass energy at the other resonances can be determined. If one could maintain the same beam orbit at all energies the only error in the mass of a resonance would be that discussed above. However, this situation can not be achieved precisely over the entire energy range of the experiment. In general, the orbit differs in length from the reference orbit by

an amount ΔL which typically ranges from +2 mm to -2 mm. ΔL is measured and corrected for by 48 horizontal beam position monitors distributed throughout the accumulator lattice.
The distribution function of the beam revolution frequency f_r is derived from an analysis of the beam current Schottky noise spectrum. The shape of the beam momentum spectrum can then be obtained if one knows the proportionality constant $\eta = (\delta f_r/f_r)/(\delta p/p)$. η depends on the accumulator lattice and was measured using a number of techniques. The error on η is estimated to be $\sim$ 10%. Reference [13] may be consulted for additional details.

8.2 The E760 Detector

The E760 detector is designed to select electromagnetic final states out of a very large hadronic background and to identify unambiguously the topology of events. A schematic of the detector is shown in Figure 10 [14]. The detector covers the complete azimuth and the laboratory polar angle from 2° to 70°. Two cylindrical scintillator arrays detect charged particles; a threshold Čerenkov counter provides electron/hadron discrimination; wire chambers provide charged particle tracking. The central and forward calorimeters provide electron and photon energy measurement and track position.
Scintillation counter hodoscope H1 consists of 8 elements of 2 mm thick NE102 scintillator lining the exterior of the 0.2 mm thick stainless steel beam pipe and covers a polar angle range from 9° to 65°. The second hodoscope H2 consists of 32 counters, each 4 mm × 3 cm × 65 cm, at a radius of 17 cm from the beamline. Since the light yield in H2 is good (50–100 photoelectrons per minimum ionizing particle), the pulse height distribution is also used to separate single charged particles from electron-positron pairs.
The Čerenkov counter is divided into eight azimuthal sectors, each covering 45°. Within each sector there are two sections covering the polar angle from 15° to 38° and 38° to 70°, respectively. Each section is equipped with mirrors focusing the Čerenkov light onto a phototube. The forward (15° to 38°) sections contain CO_2 at one atmosphere and have a pion momentum threshold of 4.9 GeV/c. The backward (38° to 70°) sections contain Freon-13 and have a pion momentum threshold of 3.7 GeV/c. Freon-13 is used in the backward sections because its higher index of refraction results in more photoelectrons per unit track length for the shorter tracks which traverse this section of the the Čerenkov counter. The light yield is strongly dependent on position, but for tracks near the center of a mirror, typically 12 photoelectrons are obtained in the forward sections and 6 photoelectrons in the backward sections.
The central calorimeter (CCAL) consists of 1280 lead-glass blocks arranged in 20 rings (polar coordinate) and 64 wedges (azimuthal coordinate) in a pointing geometry. Each block is instrumented with a photomultiplier whose output signal is digitized in an 11-bit ADC. In addition, summed output signals from matrices of 5 × 8 blocks that map the central calorimeter to a coarse $\theta - \phi$ energy grid are used in the fast trigger logic as a transverse electromagnetic energy trigger[27]. The energy resolution of this

detector is $6\%/\sqrt{E(\mathrm{GeV})}+1.4\%$. The forward calorimeter (FCAL), a lead-scintillator detector, covers polar angles from 2° to 10°.
The overall angular resolution in the detector system is $\Delta\theta$=4 mrad and $\Delta\phi$=7 mrad for charged particles. For photons, $\Delta\theta$=7 mrad and $\Delta\phi$=11 mrad. One of the wire chambers, the radial projection chamber (RPC), samples dE/dx information up to 16 times for each track providing another handle for identifying electron-positron pairs resulting from photon conversions.
The luminosity monitor[28] consists of a fixed 1 cm × 5 cm × 0.5 mm deep active volume surface barrier silicon detector mounted ≈1.5 m from the interaction region. It detects recoil protons elastically scattered at 86.5° from the beam direction. The luminosity $\mathcal{L}$ is determined by normalizing the recoil counts to the known elastic scattering cross section,

$$\mathcal{L} = N_{elastic}/[\frac{d\sigma_{elastic}}{d\Omega}d\Omega] \tag{33}$$

where $d\Omega$ is the solid angle subtended by the silicon detector. The error in the absolute measurement of the luminosity is mostly due to the error in the fit to the measured $p\bar{p}$ total cross sections in the 2.5-15.0 GeV/c region and the uncertainty in solid angle dΩ. The error due to counting statistics makes a much smaller contribution to the overall luminosity errors, which are estimated to be less than ±4%.

8.3 Trigger and Event Selection for Inclusive J/ψ Events

Reactions of the type $p\bar{p} \rightarrow J/\psi \rightarrow e^+e^- + X$, where X is a γ, π° or $\pi^+\pi^-$, have a simple topological structure containing 2 high $p_\perp$ $e^\pm$ pointing back to the interaction region. The J/ψ carries a large fraction of the antiproton momentum and, consequently, the two–body correlation between the kinematical variables of e^+ and e^- is only slightly smeared in the laboratory system and the e^+e^- and $\bar{p}$ momentum vectors are nearly coplanar. A trigger was used which selected events with both e^+ and e^- in the barrel volume.
At the fast trigger level, logic with loose constraints to select high mass objects decaying to e^+e^- was employed. The essential elements entering the trigger were logic signals from the Čerenkov cells, the scintillator hodoscopes (H1 and H2) and the matrix of 5 x 8 analog sums from the lead glass counters. The trigger required that a Čerenkov signal be associated with at least one of the two charged tracks originating from the interaction region, as defined by an appropriate coincidence between the elements of the H1 and H2 hodoscopes. Independently, two clusters in the central calorimeter are required which are separated by more than 90^0 in azimuth and which have an energy deposit which exceeds a threshold which depends on the polar angle. This trigger scheme efficiently selected ($\bar{c}c$) resonances at all energies decaying either inclusively to a J/ψ or exclusively to e^+e^-. The data were read from CAMAC using the Fermilab Smart Crate Controller [15] and ACP system [16]. The overall rate was ≤ 10 Hz and all events selected by the fast triggers could be recorded on tape without introducing a significant dead time.

Preliminary selection of inclusive J/ψ events is accomplished by requiring at least one high quality electron track, and by requiring m_{ee} to be greater than 2.0 GeV/c^2. Final event selection involves a kinematical fit to the hypothesized final state with constraints on total energy and momentum and the J/ψ mass which were treated by the method of Lagrange multipliers in the χ^2 minimization process. Additional constraints may also be imposed, depending on the final state under study. The cuts on electron quality were derived from a study of $\sim$ 4000 background-free exclusive J/ψ decays to e^+e^-.

The data were subdivided into groups of events corresponding to a nominal value of the beam energy, which was changed in small steps in order to sweep across the resonance. At each beam energy, the number of events which pass the analysis are divided by the integrated luminosity accumulated at that energy, resulting in an effective cross section as a function of energy. This is the so-called excitation curve. The resonance parameters are extracted from the excitation curve by a fit using the technique of maximum likelihood. The likelihood function to be maximized, L, is written as the product of N (= number of data points in the excitation curve) Poisson functions, each giving, for the j-th data point, the probability that n_j events be observed if ν_j are expected:

$$L = \prod_{j=1,N} \frac{\nu_j^{n_j} e^{-\nu_j}}{n_j\,!} \tag{34}$$

where:

$$\nu_j = \left[\int \mathcal{L}\, dt\right]_j \left(\sigma_{bckg} + \epsilon \int dW\; f_j(W)\sigma_{peak}\frac{\Gamma_R^2}{4\left(W - M_R c^2\right)^2 + \Gamma_R^2}\right). \tag{35}$$

The integral gives the convolution of the Breit-Wigner resonance with the center-of-mass energy distribution function $f_j(W)$, $\int \mathcal{L}\, dt$ is the integrated luminosity for each step, σ_{bckg} is the measured background cross section, ϵ is an overall acceptance–efficiency factor and:

$$\sigma_{peak} = \frac{4\pi(\hbar c)^2(2J_R+1)}{E_R^2 - 4m^2c^4} \times BR(R \to \bar{p}p) \times BR(R \to J/\psi X) \times BR(J/\psi \to e^+e^-). \tag{36}$$

The parameters determined by the fit were M_R, Γ_R and the product:

$$\Gamma(R \to \bar{p}p) \times BR(R \to J/\psi X) \times BR(J/\psi \to e^+e^-) \tag{37}$$

which is proportional to the measured area under the excitation curve and therefore depends only on one's knowledge of ϵ and $\int \mathcal{L}\, dt$ and not on the characteristics of the beam. All other quantities were input to the fit. The uncertainties on these quantities were used to estimate the systematic errors.

8.4 The χ_1 and χ_2 Charmonium States

A kinematical fit is performed on events with a topology compatible with the hypothesis

$$\bar{p}p \to \chi_{1,2} \to J/\psi\gamma \to e^+e^-\gamma. \tag{38}$$

These events included: a) events where the γ in the final state fell within the acceptance of the calorimeters and was detected and b) events where the photon escaped detection (less than 20% of the entire sample). Energy and momentum conservation and the condition that the e^+e^- come from J/ψ decay provide five constraints for type 'a' events and two for type 'b' events. An event was accepted if the probability of the fit was greater than 10^{-4}. Figure 11 shows the distribution of m_{ee} for these events at the χ_1 energy for different stages of the analysis. The shaded area corresponds to data collected outside the resonance region and normalized to an equivalent luminosity. This is the residual, non-resonant background.

Figures 12 and 13 show the measured cross section for process 38 versus the center-of-mass energy for χ_1 and χ_2, respectively. A typical center-of-mass energy distribution for the antiproton beam is shown for comparison (dashed curves). The full line represents the best fit to the data. The final results are summarized in table 4. The partial widths $\Gamma(R \to \bar{p}p)$ were obtained from the value of $[\Gamma(R \to \bar{p}p) \times BR(R \to J/\psi\gamma) \times BR(J/\psi \to e^+e^-)]$, using the published values[17] for $BR(R \to J/\psi\gamma) \times BR(J/\psi \to e^+e^-) = (1.88 \pm 0.27)\%$ at the χ_1 and $(0.93 \pm 0.14)\%$ at the χ_2.The first error given on $\Gamma(R \to \bar{p}p)$ is from the uncertainty in the measurement (statistical and systematic errors are combined in quadrature) while the second derives from the uncertainty in the branching ratios. Finally, one obtains $BR(R \to \bar{p}p)$ from the ratio of the partial width $\Gamma(R \to \bar{p}p)$ to the total width, using the correlation matrix between the two quantities to estimate the errors.

These results represent a substantial improvement over previous data. The mass measurements agree with existing measurements [17] and the errors are reduced by factors of more than two. The improvement in the total width measurements is even more substantial. Γ_{χ_1} is now measured to $\pm$ 20% whereas previously only an upper limit ($<$ 1.3 MeV with 95% C.L.) was available. An error of 10% on Γ_{χ_2} is now obtained, compared with an error of $\sim$ 40% prior to E760. The error on the partial widths, $\Gamma(\chi \to \bar{p}p)$, has also been reduced and, for the first time, a precise measurement of the $BR(\chi_1 \to \bar{p}p)$ is obtained. Reference [35] may be consulted for additional details.

Table 4: E760's results for χ_1 and χ_2

Parameters	χ_1	χ_2
M_R (MeV/c^2)	$3510.53 \pm .04 \pm .12$	$3556.15 \pm .07 \pm .12$
Γ_R (MeV)	$0.88 \pm .11 \pm .08$	$1.98 \pm .17 \pm .07$
$\Gamma(R \to \bar{p}p) \times BR(R \to J/\psi\gamma)$ $\times BR(J/\psi \to e^+e^-)$ (eV)	$1.29 \pm .09 \pm .13$	$1.67 \pm .09 \pm .12$
$\Gamma(R \to \bar{p}p)$ (eV)	$69 \pm 9 \pm 10$	$180 \pm 16 \pm 26$
$BR(R \to \bar{p}p) \times 10^4$	$(0.78 \pm .10 \pm .11)$	$(0.91 \pm .08 \pm .14)$

For the measured quantities, M_R, Γ_R and $\Gamma(R \to \bar{p}p)BR(R \to J/\psi\gamma)BR(J/\psi \to e^+e^-)$, the first errors quoted are statistical and the second are systematic.

8.5 Comparison of the χ States with Theoretical Predictions

a. Hadronic Widths

Predictions for the hadronic widths of the χ states have been calculated to the lowest order and, for χ_0 and χ_2, first order corrections (in square brackets below) have been estimated [18, 45]:

$$\Gamma(\chi_0 \to gg) \simeq \left(6\alpha_s^2 \mid R'_p(0) \mid^2 / m_c^4\right) \times (1 + [9.5\alpha_s/\pi]) \tag{39}$$

$$\Gamma(\chi_1 \to q\bar{q}g) \simeq \left(\frac{8}{9\pi} n_f \, \alpha_s^3 \mid R'_p(0) \mid^2 / m_c^4\right) \times ln\,(m_c < r >) \tag{40}$$

$$\Gamma(\chi_2 \to gg) \simeq \left(\frac{8}{5}\alpha_s^2 \mid R'_p(0) \mid^2 / m_c^4\right) \times (1 - [2.2\alpha_s/\pi]) \tag{41}$$

where $\alpha_s \equiv \alpha_s(m_c)$ is the running coupling 'constant' of the strong interactions calculated at the effective c–quark mass value $m_c = 1.5$ GeV/c^2 , $n_f = 3$ is the number of light flavors, $< r >= 3.17$ GeV^{-1} is the confinement radius and $\mid R'_p(0) \mid$ is the first derivative of the radial wave function at the origin for the $(c\bar{c})$ system in a P-state
$\mid R'_p(0) \mid$ has been estimated by solving the Schrödinger equation with a phenomenological central potential; its numerical value depends strongly on the functional shape of the potential [21]. The hadronic widths can be written as:

$$\Gamma_{had} \simeq \Gamma_R - \Gamma_R(\chi \to J/\psi\gamma) = \Gamma_R(1 - BR(\chi \to J/\psi\gamma)).$$

Inserting the known values [17] of the branching ratios for radiative decays one obtains from the measurements:

$$\Gamma_{had} = (0.64 \pm 0.11) \text{ MeV for } \chi_1 \text{ and } \Gamma_{had} = (1.71 \pm 0.21) \text{ MeV for } \chi_2.$$

In addition, one takes from the literature [22] : $\Gamma(\chi_0 \to gg) \simeq \Gamma_{\chi_0} = 13.5 \pm 5.3$ MeV. To lowest order, the ratio between $\Gamma(\chi_0 \to gg)$ and $\Gamma(\chi_2 \to gg)$ is independent of the wave function of the $(c\bar{c})$ state and of the value of α_s; $\Gamma(\chi_0 \to gg)/\Gamma(\chi_2 \to gg) = 15/4$. When first order radiative corrections are included, using for α_s the value [18] $0.276 \pm .014$ one obtains from equation 39 and 41:

$$\Gamma(\chi_0 \to gg)/\Gamma(\chi_2 \to gg) = \frac{15}{4} \times (2.27 \pm 0.08) = 8.53 \pm 0.30$$

which should be compared to the experimental value of 7.9 ± 3.9, where the large error comes from the uncertainty on Γ_{χ_0}
If one uses the quoted value of α_s, one estimates from the value of $\Gamma(\chi_2 \to gg)$ $|R'_p(0)|^2 = 0.088 \pm 0.012$ GeV^5. This should be compared to the theoretical predictions [21] which vary from 0.057 to 0.11 GeV^5 , depending on the functional form of the potential.
It is also interesting to compare the measurement for the $\Gamma(\chi_1 \to q\bar{q}g)$ with the theoretical calculation which, in this case, stops at the lowest order (40). Using

again the same value for α_s and the value of $|R'_p(0)|^2$ derived from $\Gamma(\chi_2 \to gg)$, one obtains $\Gamma(\chi_1 \to q\bar{q}g) \sim 0.50$ MeV to be compared with the experimental value of (0.64 ± 0.11) MeV.

b. Radiative widths.

Precise estimates of the widths for electric dipole $P \to S$ transitions can be obtained by combining the known branching ratios [17] and the measured values for the total widths of χ_1 and χ_2. The radiative widths, given in table 5, are at the low end of theoretical predictions[23]. The relative magnitude of the two partial widths is compatible with the expected E_γ^3 scaling law.

Table 5: Radiative transition widths of χ_1 and χ_2 from E760

	Γ_γ^{exp} (keV)	$(\Gamma_\gamma^{exp}/E_\gamma^3) \times 10^9$ (MeV^{-2})
χ_1	240 ± 40	$4.08 \pm .70$
χ_2	267 ± 33	$3.36 \pm .42$

8.6 The $^1P_1$ State of Charmonium

In $\bar{p}p$ annihilations the $^1P_1$ state can be formed through coherent annihilation into three hard gluons (the annihilation into two gluons violates C-parity). The $^1P_1$ is expected to be narrow (≤ 1.0 MeV) and the dominant decay mode is expected to be the electric dipole transition to the $\eta_c\gamma$ final state[31]. Several predictions of the mass of the singlet P can be found in the literature[32], most of them within a few MeV of the center-of-gravity of the $\chi_c(^3P_J)$ states, defined as:

$$m_{c.o.g.} = \frac{m_{\chi_0} + 3m_{\chi_1} + 5m_{\chi_2}}{9} = 3525.27 \pm 0.12 \text{ MeV} \tag{42}$$

where the mass of the χ_0 was obtained from the Particle Data Book compilation [17] and the masses of the $\chi_{1,2}$ are taken from E760's measurements [35].
The cross section at the peak of the resonance for the formation reaction $\bar{p}p \to^1 P_1$ is expected to be $\leq 10^{-6}$ of the total cross section for $\bar{p}p \to$ hadrons. To maximize the chances of successfully identifying this rare process in the presence of a large hadronic background, the decay of the $^1P_1$ into the following electromagnetic final states has been searched for:

$$^1P_1 \to \eta_c + \gamma \to (\gamma\gamma) + \gamma \tag{43}$$

$$^1P_1 \to J/\psi + \pi^\circ \to (e^+e^-) + \pi^\circ \tag{44}$$

$$^1P_1 \to J/\psi + \pi + \pi \to (e^+e^-) + \pi + \pi. \tag{45}$$

While the dominant decay mode is expected to be $\eta_c\gamma$, the small branching ratio for $\eta_c \to \gamma\gamma$ strongly suppresses the 3γ final state leaving it comparable in rate to 44 and

45, but with significantly more background. The branching ratios for decays 44 and 45 are expected to be small since reaction 44 does not conserve isospin and reaction 45 is suppressed by the limited phase space available and by angular momentum barrier effects. However, because they include a pair of electrons with large invariant mass, the final state signatures for these decays are highly distinctive and permit a sensitive search for the $^1P_1$. Only the decay channels 44 and 45 will be discussed here.

The search for the $^1P_1$ was confined to the immediate vicinity of $m_{c.o.g.}$ (42). Data were taken in small energy steps ($\leq$ 500 keV) with an integrated luminosity of $\sim$ 1000 nb^{-1} at each step to allow observation of a narrow resonance with a small cross section.

A mass plot of the e^+e^- invariant mass is shown in figure 14 for data taken in the vicinity of $m_{c.o.g.}$ and, for comparison, data taken at the ψ' resonance. It is clear that events of the type $\bar{p}p \rightarrow J/\psi + X$ are present in the data. It should be noted that the event rate for this data is much smaller than that for the ψ'. This explains why the background component appears to be larger. Events of Figure 14 with $m_{e^+e^-} > 2.9\mathrm{GeV/c^2}$ were fitted to reactions 44, 45, to $\bar{p}p \rightarrow J/\psi + \gamma \rightarrow e^+e^-\gamma$ and to $\bar{p}p \rightarrow e^+e^-$ whenever the event topology was compatible with the final state hypothesis. Most of the events could be fitted either to $J/\psi + \gamma$, or to $J\psi + \pi^\circ$. The shaded areas in Figure 14 represent events fitted to $\bar{p}p \rightarrow J/\psi + \pi^\circ$ (black solid), $\bar{p}p \rightarrow J/\psi + \gamma$ (cross hatched) and $\bar{p}p \rightarrow e^+e^-$ (vertical stripes). The residual events in the J/ψ mass band are compatible with what is expected for the background. No events were found to fit the reactions $\bar{p}+p \rightarrow J/\psi + \pi^\circ + \pi^\circ$ or $\bar{p}+p \rightarrow J/\psi + \pi^+ + \pi^-$. C conservation prevents the $J^{PC} = 1^{+-}$ singlet P state from decaying into $J/\psi + \gamma$. The events observed in this channel can therefore be due only to a true continuum or due to the contributions of the nearby $\chi_1(3510.6)$ and $\chi^2(3556.0)$ resonances. The measured cross section is found to be consistent with the latter hypothesis when the shape of the beam distribution, with its low momentum tail, is taken into account.

The final results for the $\bar{p}p \rightarrow J/\psi + \pi^\circ \rightarrow e^+ + e^- + \gamma + \gamma$ channel are shown in figure 15. The data is binned in intervals of 150 keV in the center-of-mass energy, with overlapping bins added. One notices that below $m_{c.o.g.}$ an apparently uniform level of ≈ 2.0 events/pb^{-1} is observed. This corresponds to a cross section of $\sigma(\bar{p}p \rightarrow J/\psi + \pi^\circ)$ = (99 $\pm$ 40) pb, in reasonable agreement with what is expected for the continuum [33]. Above $m_{c.o.g}$ a consistently higher cross section is observed in the small region around 3526 MeV.

The data of the $^1P_1$ scan were analyzed with the maximum likelihood method by fitting the measured cross section to a constant continuum level plus a Breit-Wigner resonance function convoluted with the known beam momentum shape. The ratio of L(H_1), the maximum value of the likelihood function for the hypothesis tested (resonance plus background) to the maximum value, L(H_0), of the likelihood function for the null hypothesis (no resonance) yields $\lambda_0 = [(2ln[L(H_1)/L(H_0)])]^{1/2} = 3.5$. Since the use of the likelihood ratio to extract a confidence level may be questionable for data with small statistics, the probability that an 'accidental' resonance structure may result from a fluctuation of a constant background has been estimated, by performing several thousand Monte Carlo simulations of the event distribution (using the actual energies and luminosities) assuming a constant cross section equal to the average of

all the measurements. By analyzing the data of the Monte Carlo 'experiments' with exactly the same procedure used in analyzing the real data, it was found that the probability of a structure with $\lambda \geq \lambda_o$ arising from a statistical fluctuation anywhere in the scanned region is only 1 in 400.
Based on this analysis, E760 claims evidence of a narrow resonant structure in the $\bar{p}p \rightarrow J/\psi + \pi^\circ$ channel, with a resonance mass value M_R=3526.2±.2 MeV/c^2. Because of the low available statistics of the experiment and the $\sim$ 750 keV width of the beam distribution, only an upper limit can be set on the resonance width of $\Gamma_R \leq$1.1 MeV at a 90% confidence level. The product of the branching ratios depends on Γ_R. If one takes as a plausible range of values 1000 keV$\geq \Gamma_R \geq$ 500 keV, one obtains:

$$(1.6 \pm 0.4) \times 10^{-7} \leq BR(R \rightarrow \bar{p}p)BR(R \rightarrow J/\psi + \pi^\circ) \leq (2.1 \pm 0.6) \times 10^{-7}$$

after folding in the value BR($J/\psi \rightarrow e^+e^-$) = (6.9 ± 0.9) [17]. This structure is interpreted to be the 1^1P_1 state of charmonium. Reference [36] may be consulted for additional details.

8.7 Comparision of the $^1P_1$ Data with Theoretical Predictions

A limit of BR($^1P_1 \rightarrow J/\psi\pi\pi$)/ BR($^1P_1 \rightarrow J/\psi\pi^\circ$)$\leq$ 0.25 at the 90% confidence level is set since no di-pion events are observed. This would seem to conflict with the prediction of Kuang, Tuan and Yan who predict BR($^1P_1 \rightarrow J/\psi\pi\pi$) to be similar to BR($^1P_1 \rightarrow J/\psi\pi^0$) [34]. If one extends the calculation of Voloshin from the $b\bar{b}$ system to the charmonium system, this would seem to be in better agreement with the data [37].
The mass obtained by E760 for the $^1P_1$ is consistent with the one-loop QCD correction calculations which depend only on the value of $\alpha_s(m_c)$ and the radial wavefunction [20].

8.8 R704 and the $^1P_1$

R704 reported 5 inclusive J/ψ events near $m_{c.o.g}$ [24]. The 5 events were interpreted as a possible hint of the $^1P_1$ resonance, though the authors conceded that the 5 events were also compatible with background. In view of the recent E760 results, it is interesting to take a second look at the R704 data.
It should first be pointed out that E760 has an acceptance which is 7.5 times larger than R704 for the reaction $\bar{p}p \rightarrow J/\psi + X \rightarrow e^+e^- + X$. Unlike R704, E760 has the capability to fully reconstruct the decay $J/\psi \rightarrow e^+ + e^- + \gamma + \gamma$. E760's sensitivity for detecting the $^1P_1$ in this mass range is $\sim$100 times larger than that of R704.
A comparison of the masses obtained by E760 and R704 indicate that they are separated by $\sim 2\sigma$. This is determined after normalizing the mass scales of the two experiments based on their respective measurements of the masses of the χ_1 and χ_2 states. A comparison of the cross sections of the two experiments indicates that if the 5 events seen by R704 were to be interpreted as a resonance, the cross section for

the formation of that resonance would be ~ 13.5 times larger than the cross section measured by E760. If the R704 results are correct, E760 should have measured 540 signal events rather than the 40 observed events. Finally, the 5 events observed by R704 are entirely compatible with the non-resonant background measured by E760, an interpretation which was never excluded by R704.

8.9 Trigger and Event Selection for $\gamma\gamma$ Final States

E760's neutral trigger consists of two levels. At the hardware level a topological trigger requires at least two energetic clusters in the central calorimeter separated by $\geq 90°$ in azimuth [27]. Events with charged particles are vetoed by requiring no hits in the H1 or the forward veto scintillation counters. The calorimeter data are read into online processors [16] which compute the invariant masses of all photon pairs ($M_{\gamma\gamma}$) and the total energy deposited in the calorimeters. Events with any $M_{\gamma\gamma} \geq 2.0\ GeV/c^2$ are recorded on tape.

The $\gamma\gamma$ analysis begins with events with two central calorimeter clusters with invariant mass $M_{\gamma\gamma} \geq 2.5\ GeV/c^2$. Additional low energy clusters are allowed in the central calorimeter to protect against rate-dependent pile-up effects. No clusters are allowed in the forward calorimeter. A 4C kinematical fit to the $\gamma\gamma$ hypothesis is performed and events with a fit probability $CL \leq 5 \times 10^{-3}$ are rejected. An invariant mass cut at $\pm 10\% \sqrt{s}$ is imposed, corresponding to a 3σ cut on the mass resolution as inferred from $J/\psi \rightarrow e^+e^-$ and $\psi' \rightarrow e^+e^-$ events. Masses calculated by pairing any additional low energy clusters with each of the high energy clusters associated with the $\gamma\gamma$ candidate are formed. Events with any mass in the π° $(80-170\ MeV/c^2)$ or η $(410-690\ MeV/c^2)$ window are rejected. Due to the rapid increase of the background with $|cos\theta^*|$ the acceptance for the $\gamma\gamma$ channels is restricted to near 90 degrees. The exact cut on $|cos\theta^*|$ depends on the state under study.

8.10 $\chi_2 \rightarrow \gamma\gamma$

The final data set for the reaction $p\bar{p} \rightarrow \gamma\gamma$ is shown in figure 16 for the region around the χ_2 resonance. $|cos\theta^*|$ has been restricted to values less than 0.40 in this analysis. The angular distribution for the reaction $\bar{p}p \rightarrow \chi_2 \rightarrow \gamma\gamma$ is needed in order to extract the partial width $\Gamma(\chi_2 \rightarrow \gamma\gamma)$ from a measurement over the restricted angular region $|cos\theta^*| \leq 0.40$. Reference [51] may be consulted for details.

Correcting the results for efficiency and acceptance one finds that:

$$BR(\chi_2 \rightarrow \bar{p}p)BR(\chi_2 \rightarrow \gamma\gamma) = (1.69 \pm 0.38 \pm 0.14) \times 10^{-8}$$

$$BR(\chi_2 \rightarrow \gamma\gamma) = (1.54 \pm 0.40 \pm 0.24) \times 10^{-4}$$

$$\Gamma(\chi_2 \rightarrow \gamma\gamma) = (304 \pm 84 \pm 49)\ eV.$$

E760's measurements of $BR(\chi_2 \rightarrow \bar{p}p) = (0.91 \pm 0.08 \pm 0.14) \times 10^{-4}$ and $\Gamma(\chi_2) = 1.98 \pm 0.17 \pm 0.07$MeV [35] have been used to obtain the last two values.

8.11 Comparison of $\chi_2 \to \gamma\gamma$ data with Theoretical Predictions

Perturbative QCD expressions for the decay rates of charmonium into gluons and photons with next-to-lowest order corrections can be found in [45]. The strong coupling constant $\alpha_s(m_c)$ can be derived from the ratio

$$\frac{\Gamma(\chi_2 \to gg)}{\Gamma(\chi_2 \to \gamma\gamma)} = \frac{9\alpha_s^2}{8\alpha^2}\left[\frac{1-2.2\alpha_s/\pi}{1-16\alpha_s/3\pi}\right]. \tag{46}$$

Using E760's value of $\Gamma(\chi_2 \to gg) = 1.71 \pm 0.21$ MeV [35], a value $\alpha_s(m_c) = 0.36 \pm 0.04$ is obtained from the expression above. It should be noted that the lowest order correction to the two photon annihilation rate of the χ_2 is very large, $[1-16\alpha_s/3\pi] = 0.49$ for $\alpha_s = 0.3$ and that potentially large relativistic corrections have not been taken into account. A comparison of E760's results with previous measurements and with theoretical predictions appears in table 6. The branching ratio and partial width are both significantly smaller than the theoretical predictions, indicating that higher order QCD corrections and relativistic corrections are probably necessary to fully understand this result.

Table 6: Comparison of experimental and theoretical results for $\chi_2 \to \gamma\gamma$

	$\Gamma(\chi_2 \to \gamma\gamma)$ (KeV)	$B\bar{R}(\chi_2 \to \gamma\gamma) \times 10^{-4}$
Experiment		
E760	$0.30 \pm 0.08 \pm 0.05$	$1.5 \pm 0.4 \pm 0.2$
R-704 [40][1]	$2.9^{+1.3}_{-1.0} \pm 1.7$	$11^{+5}_{-4} \pm 4$
CLEO [42]	< 1.0 (95% CL)	
TPC [43]	< 4.2 (95% CL)	
DASP [17]	< 1.6 (90% CL)	
Theory		
PQCD [45][2]	0.70 ± 0.13	
B.A. [39]	0.56	
B.B.L. [46]		4.1 ± 1.1 ($\pm 36\%$)

[1] Uses isotropic angular distribution and $\Gamma(\chi_2) = 2.6^{+1.4}_{-1.0}\ MeV$.
[2] Using $\Gamma(\chi_2 \to gg) = 1.71 \pm 0.21\ MeV$.

8.12 $\eta_c \to \gamma\gamma$

The final data set for the reaction $p\bar{p} \to \gamma\gamma$ is shown in figure 17 for the region around the η_c resonance. $|cos\theta^*|$ has been restricted to values less than 0.20 in this analysis in order to maximize the signal-to-background. The resonance parameters obtained from a preliminary analysis of this data are:

$$\sigma(\bar{p}p \to \eta_c \to \gamma\gamma) = 54.7 \pm 14.5 \pm 9.3 \text{ pb} \tag{47}$$

$$M = 2989.9 \pm 2.2 \pm 0.4 \text{ MeV} \tag{48}$$

$$\Gamma = 15.5 \pm 6.8 \pm 6.4 \text{ MeV}. \tag{49}$$

Correcting the measured cross section for efficiency and acceptance:

$$BR(\eta_c \to \bar{p}p)BR(\eta_c \to \gamma\gamma) = (41.7 \pm 11.2 \pm 7.5) \times 10^{-8} \tag{50}$$

$$BR(\eta_c \to \gamma\gamma) = (3.47 \pm 1.49 \pm 0.63) \times 10^{-4} \tag{51}$$

$$\Gamma(\eta_c \to \gamma\gamma) = (5.4 \pm 3.3 \pm 1.0) \text{ keV}. \tag{52}$$

The Particle Data Group [17] value of $BR(\eta_c \to \bar{p}p) = (12 \pm 4) \times 10^{-4}$ has been used to obtain the last two values.

8.13 Comparison of $\eta_c \to \gamma\gamma$ data with Theoretical Predictions

The lowest order prediction for $\eta_c \to \gamma\gamma$ is [10]:

$$\Gamma(\eta_c \to \gamma\gamma) = \frac{3\alpha^2 e_Q^4 |R(0)|^2}{M^2}. \tag{53}$$

$R(0)$ can be obtained from the leptonic width [52]:

$$\Gamma(J/\psi \to e^+e^-) = \frac{4\alpha^2 e_Q^2}{M^2}|R(0)|^2. \tag{54}$$

Making the appropriate substitutions, one arrives at

$$\Gamma(\eta_c \to \gamma\gamma) = \frac{4}{3}\Gamma(J/\psi \to e^+e^-) = 6.3 \text{ keV}. \tag{55}$$

Applying first order QCD corrections results in $\Gamma(\eta_c \to \gamma\gamma)$ =7.5 keV [49]. A comparison of these results with previous measurements and with some theoretical predictions appears in table 7. Unfortunately, the experimental results are not of sufficient precision to differentiate between theories.
To lowest order, the expression for the hadronic width of the η_c is [47]:

$$\Gamma(\eta_c \to gg) = \frac{8\pi}{3M^2}\alpha_s^2|\psi(0)|^2. \tag{56}$$

This can be related to the hadronic width of the J/ψ:

$$\Gamma(J/\psi \to ggg) = \frac{40(\pi^2 - 9)}{81M^2}\alpha_s^3|\psi(0)|^2. \tag{57}$$

When this is combined with higher order corrections [49] the result is

$$\Gamma(\eta_c \to gg) = (173 \pm 10)\Gamma(J/\psi \to ggg) \tag{58}$$

or

$$\Gamma(\eta_c) \sim (8.3 \pm 0.5) \text{ MeV}. \tag{59}$$

Table 7: Comparison of experimental and theoretical results for $\eta_c \to \gamma\gamma$

	$\Gamma(\eta_c \to \gamma\gamma)$ (keV)	$BR(\eta_c \to \gamma\gamma) \times 10^{-4}$
Experiment		
E760[a]	$3.6 \pm 2.0 \pm 0.6$[b]	$3.5 \pm 1.5 \pm 0.6$
R704 [41]		$6^{+4}_{-3} \pm 4$
CLEO [42]	$5.9^{+2.1}_{-1.8} \pm 1.9$	
TPC [43]	$6.4^{+5.0}_{-3.4}$	
PLUTO [50]	28 ± 15	
Theory		
PQCD [45]	3.7 ± 1.4	
B.A. [39]	4.8	

9 Conclusion

The first great strides in charmonium physics were made at e^+e^- machines where the properties of the 1^{--} states were determined with good accuracy allowing for the development and testing of a great many theoretical calculations. The next great step has been the precise study of states with other quantum numbers in $p\bar{p}$ interactions. Measurements of the χ_1 and χ_2 resonances have been made with a precision not possible elsewhere. More importantly, the long sought after $^1P_1$ state has been discovered. Good measurements of the η_c have been made, with better measurements to follow when improved statistics are available.

The important experimental tasks which remain in charmonium physics have been reduced to confirming the Crystal Ball's result for the η_c' (or finding the η_c' elsewhere), confirming the $^1P_1$ result of E760 and seeing the $^1P_1$ decay to another channel, accurately measuring the η_c, and discovery of the D-states. The next generation of the E760 experiment at Fermilab, E835, will attempt to cover as much of this ground as possible in 1995. Should SuperLear ever be built at CERN, much of its attention will also be focussed on these issues.

Heavy quarkonium states are QCD laboratories. If the quarks are heavy enough the bound system should behave more or less non-relativistically allowing a wealth of information to be obtained by solving the non-relativistic Schrödinger equation. Unfortunately, charmonium can not be treated as an entirely non-relativistic system and relativistic corrections are often necessary. $b\bar{b}$ bound states, on the other hand, begin to approach a mass scale which is truly non-relativistic. Bottomonium poses a much more difficult challenge to experimentalists than charmonium. The $p\bar{p}$ resonance formation cross section scales as p_{cm}^{-2} of the $\bar{p}$ beam. States which are difficult to produce at charmonium energy scales become even more difficult to produce in the $b\bar{b}$ regime. A very high luminosity source of $p\bar{p}$ interactions along with a very fast, very smart trigger will be required in order to have any chance at all of applying this technique to $b\bar{b}$ physics. There are those who have already begun to contemplate such experiments [53]. If they are successful, they will no doubt continue a long standing

tradition of extracting detailed and fundamental physics from a thorough study of a two-body bound state.

10 Acknowledgements

I must thank my E760 collaborators, without whom none of this work would have been possible. I would like to thank Professor D. C. Peaslee for his efforts in organizing the Hadron 92 Summer School and I would like to thank Professor S. F. Tuan for useful conversations and for preprints of his papers dealing with $^1P_1$ physics. Finally, I would like to extend my gratitude to Mika Masuzawa and Jack Zhao, both from E760, for their help in preparing this manuscript.

References

[1] J. D. Bjorken and S. L. Glashow, Phys. Lett., 11, 255 (64).

[2] N. Cabibbo, Phys. Rev. Lett. 10, (1963) 531.

[3] S. L. Glashow, J. Iliopoulos and L. Maiani, Phys. Rev. D2, (1970) 1285.

[4] J. J. Aubert et al, Phys. Rev. Lett. 33 (1974) 1404.

[5] J. E. Augustin et al, Phys. Rev. Lett. 33 (1974) 1406.

[6] C. Bacci et al, Phys. Rev. Lett. 33 (1974) 1408.

[7] S. Okubo, Phys. Lett. 5 (1963) 165, G. Zweig, unpublished. Cern Preprints, Th 401, 412 (1964), J. Iizuka, Suppl. Progr. Theor. Phys. 37-38 (1966) 21.

[8] G. Goldhaber et al, Phys. Rev. Lett. 37 (76) 255.

[9] J. E. Wiss et al, Phys. Rev. Lett. 37 (76) 1531.

[10] V. A. Novikov et al, Physics Reports C41 (78) 1.

[11] C.N. Yang, Phys. Rev. 77 (1950) 242.

[12] C. Baglin et al., CERN-EP Internal Report 85-01 (85); C. Baglin et al., Phys. Lett. B171 (86) 135; C. Baglin et al., Nucl. Phys. B286 (87) 592; C. Baglin et al., Phys. Lett. B187 (87) 191; C. Baglin et al., Phys. Lett. B231 (89) 557.

[13] T. A. Armstrong et al., Phys. Rev. D47 (93) 772.

[14] C. Biino et al., Nucl. Inst. Methods A271 (88) 417; C. Biino et al., IEEE Trans. Nucl. Sci. 36 (89) 98; R. Calabrese et al., Nucl. Inst. Methods A277 (89) 116; R. Calabrese et al., IEEE Trans. Nucl. Sci. 36 (89) 54; L. Bartoszek et al., Nucl. Inst. Methods A301 (91) 47; M. A. Hasan et al., Nucl. Inst. Methods A295 (90) 73.

[15] S. Hansen et al., IEEE Trans. Nucl. Sci. 34 (87) 1003.

[16] I. Gaines et al., Comp. Phys. Commun. 45 (87) 323; C. Gay et al., IEEE Trans. Nucl. Sci. 34 (87) 870.

[17] Review of Particle Properties, Particle Data Group, Phys. Lett. B239 (90) and references therein.

[18] R. Barbieri et al., Nucl. Phys. B192 (81) 61

[19] R. H. Dalitz and S. F. Tuan, in Proceedings of the 10th Hawaii Conference in High Energy Physics, Honolulu, Hawaii, (95) 707.

[20] F. Halzen et al., Phys. Lett. B283 (92) 379.

[21] M. G. Olsson et al., Phys. Rev. D31 (85) 81.

[22] J.E. Gaiser et al., Phys. Rev. D34 (86) 711.

[23] E. Echten et al., Phys. Rev. D21 (80) 203; P. Moxhay and J. L. Rosner, Phys. Rev. D28 (83) 1132; R. McClary and N. Byers, Phys. Rev. D28 (83) 1692; S. N. Gupta, W. W. Repko and C. J. Suchyta III, Phys. Rev. D39 (89) 974.

[24] C. Baglin et al., Phys. Lett. B171 (86) 135.

[25] J. Peoples Jr., Proceedings of the Workshop on the Design of a low Energy Antimatter Facility, ed. D. Cline, (World Scientific Publishing Co., Singapore, 1989), p964.

[26] D. Möhl et al., Phys. Rep. 58 (80) 73.

[27] R. Ray, J. L. Rosen, M. Masuzawa and J. Zhao, Nucl. Inst. Methods A307 (91) 254.

[28] M. Sarmiento et al., "A Luminosity Monitor for FNAL Experiment E760," to be submitted to Nucl. Inst. Methods.

[29] C. Edwards et al., Phys. Rev. Lett. 48 (82) 70.

[30] E. D. Bloom and C. W. Peck Annu. Rev Nucl Part. Sci. 33 (83) 143

[31] R. McClary and N. Byers, Phys. Rev. D28 (83) 1692; V. O. Galkin et al., Sov. J. Nucl. Phys. 51 (90) 705.

[32] J. Pantaleone and S. H. Tye, Phys. Rev D37 (88) 3337; S. N. Gupta et al., Phys. Rev. D39 (89) 974; V. V. Dixit et al., Phys. Rev. D42 (90) 166; A. M. Badalyan and V. P. Yurov, Phys. Rev. D42 (90) 3138; L. P. Fulcher, Phys. Rev. D44 (91) 2079; J. Stubbe and A. Martin, Phys. Lett. B271 (91) 208; Y. Q. Chen and Y. P. Kuang, Phys. Rev. D46 (92) 1165; F. Halzen et al., Phys. Lett. B283 (92) 379 D. B. Lichtenberg and R. Potting, Phys Rev D46 (92) 2150.

[33] M. K. Gallard et al., Phys. Lett. 110B (82) 489.

[34] Y. P. Kuang, S. F. Tuan and T. M. Yan, Phys. Rev. D37 (88) 1210.

[35] T. A. Armstrong et al., Nucl. Phys. B373 (92) 35.

[36] T. A. Armstrong et al., Phys. Rev. Lett. 69 (92) 2337.

[37] M. B. Voloshin, Sov. J. Nucl. Phys. 43 (86) 1011.

[38] Z. P. li et al., Phys. rev. D43 (91) 2161;

[39] T. Barnes and E. Ackleh, ORNL-CCIP-92-05, UTK-92-3.

[40] C. Baglin et al., Phys. Lett. B187 (87) 191.

[41] C. Baglin *et al.*, Phys. Lett. B **231**, 557 (1987).

[42] W. Chen et al., Phys. Lett. B243 (90) 169.

[43] Uehara et al., Phys. Lett. B266 (91) 188.

[44] H. Aihara *et al.*, Phys. Rev. Lett. **60**, 2355 (1988).

[45] W. Kwong et al., Phys. Rev. D37 (88) 3210.

[46] G. Bodwin et al., Phys Rev. D46 (92) 1914.

[47] W. Kwong, J. L. Rosner and C. Quigg, Ann. Rev. Part. Sci. 37 (87) 325.

[48] M. G. Olsson et al., Phys. Rev. D31 (85) 1759.

[49] R. Barbieri et al., Phys. Lett. B106 (81) 497.

[50] C. Berger et al., Phys. Lett. B167 (86) 120.

[51] T. A. Armstrong et al., FERMILAB-Pub-92/266-E.

[52] R. VanRoyen and V. F. Weisskopf, Nuovo Cimento 50A (67) 617, R. VanRoyen and V. F. Weisskopf, Nuovo Cimento 51A (67) 583.

[53] P. Dalpiaz, Private communication.

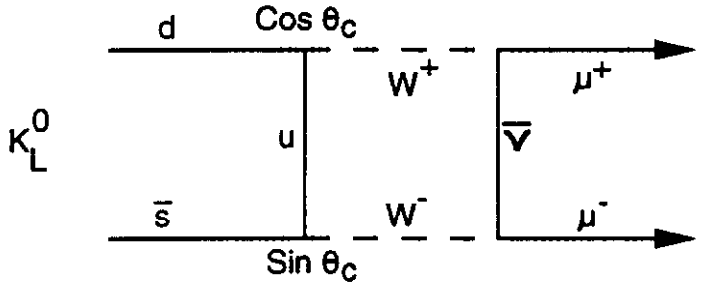

Figure 1. Quark diagram for K_L decay to 2 muons with only u, d and s quarks.

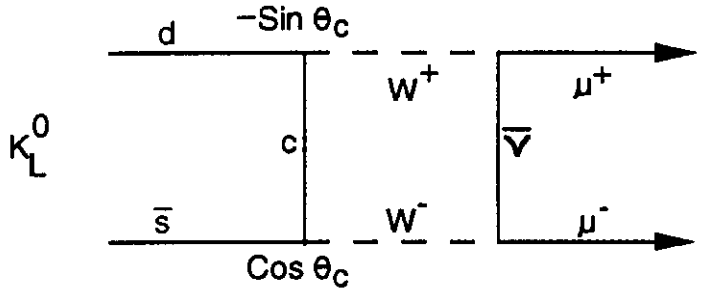

Figure 2. Cancelling quark diagram for K_L decay to 2 muons in the GIM model.

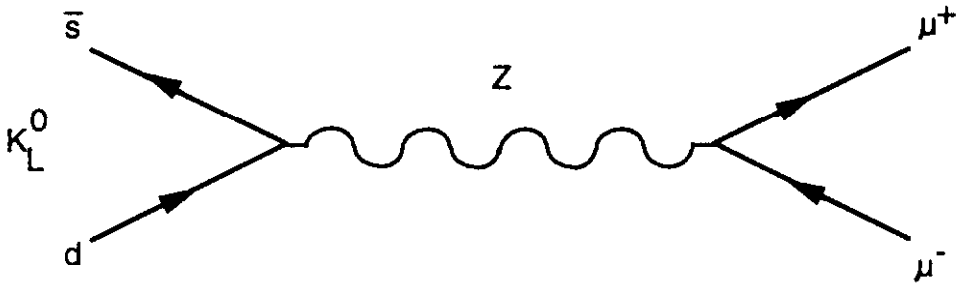

Figure 3. Diagram for K_L decay to 2 muons.

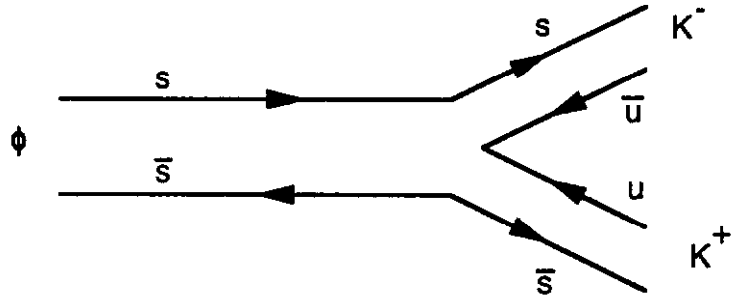

a)

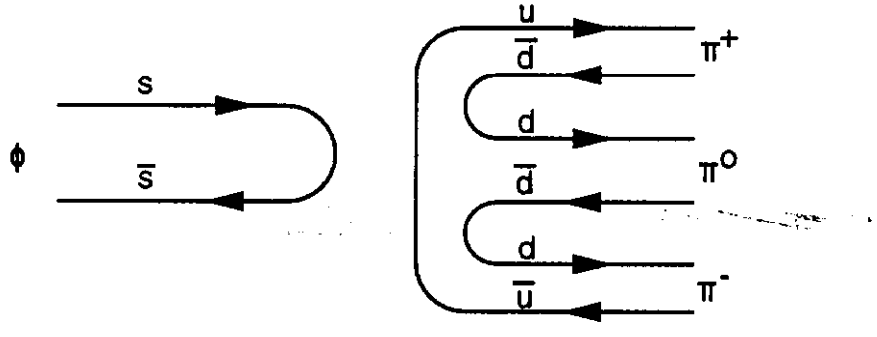

b)

Figure 4. OZI allowed a) and OZI forbidden b) decay diagrams for the ϕ.

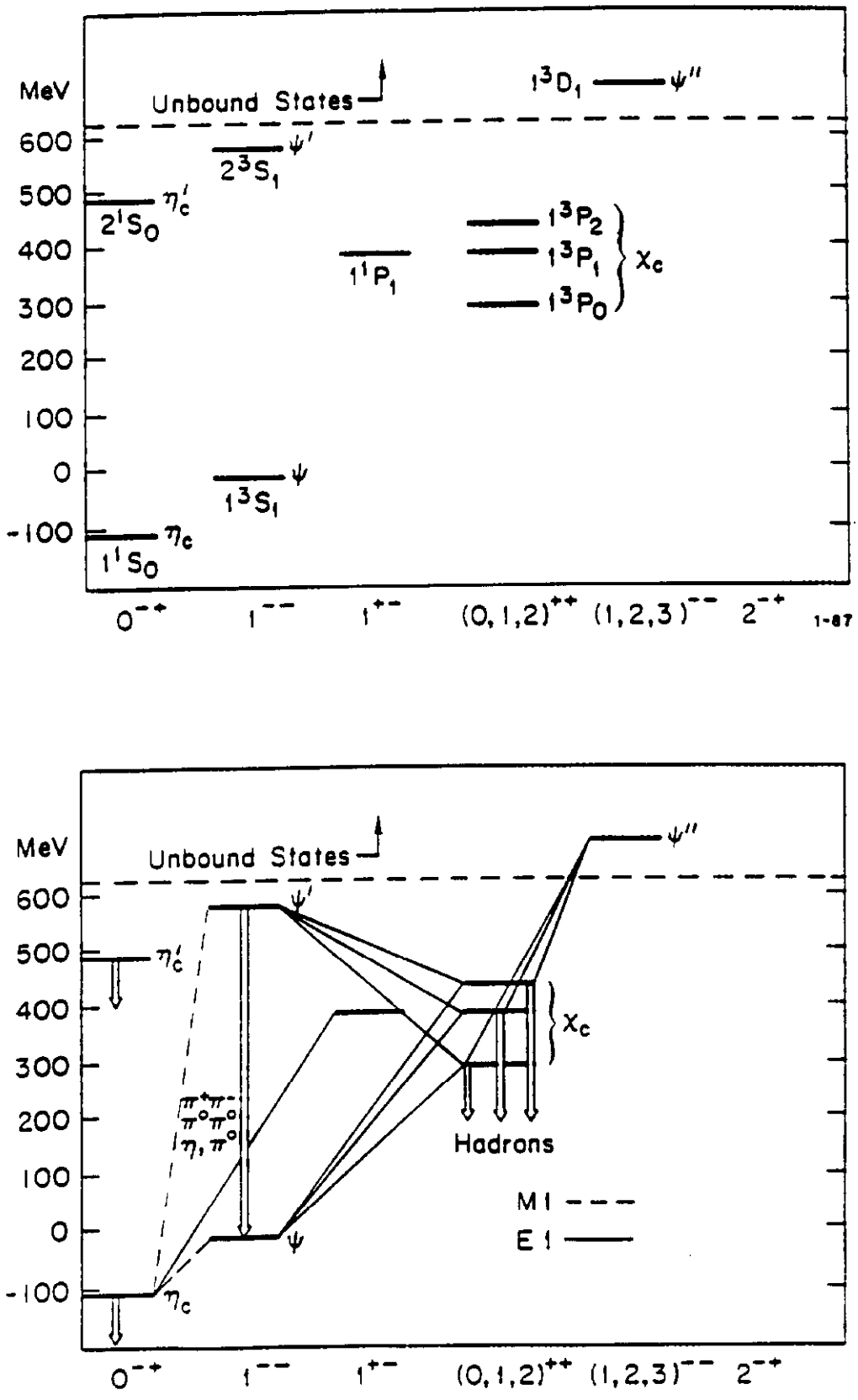

Figure 5. Level diagram for charmonium. Shown on the lower plot are the radiative and hadronic transitions.

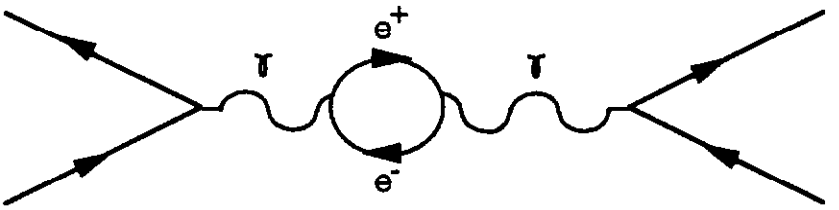

Figure 6. QED vacuum polarization diagram.

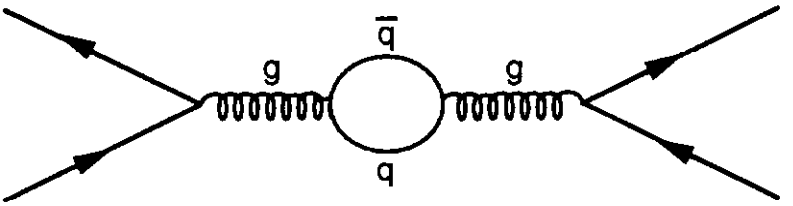

Figure 7. Screening due to a quark-antiquark loop in QCD.

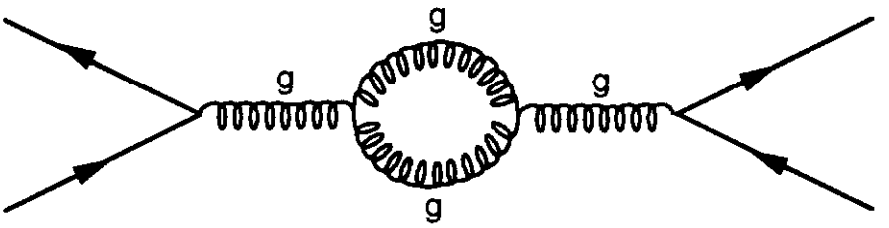

Figure 8. Antiscreening due to gluon loops in QCD.

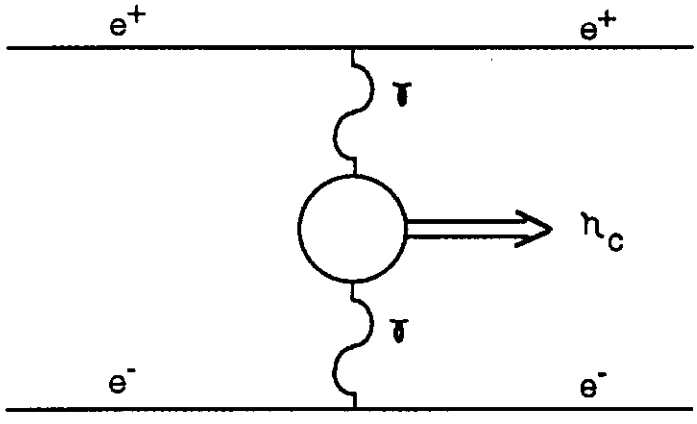

Figure 9. Two photon production of η_c in e^+e^- interactions.

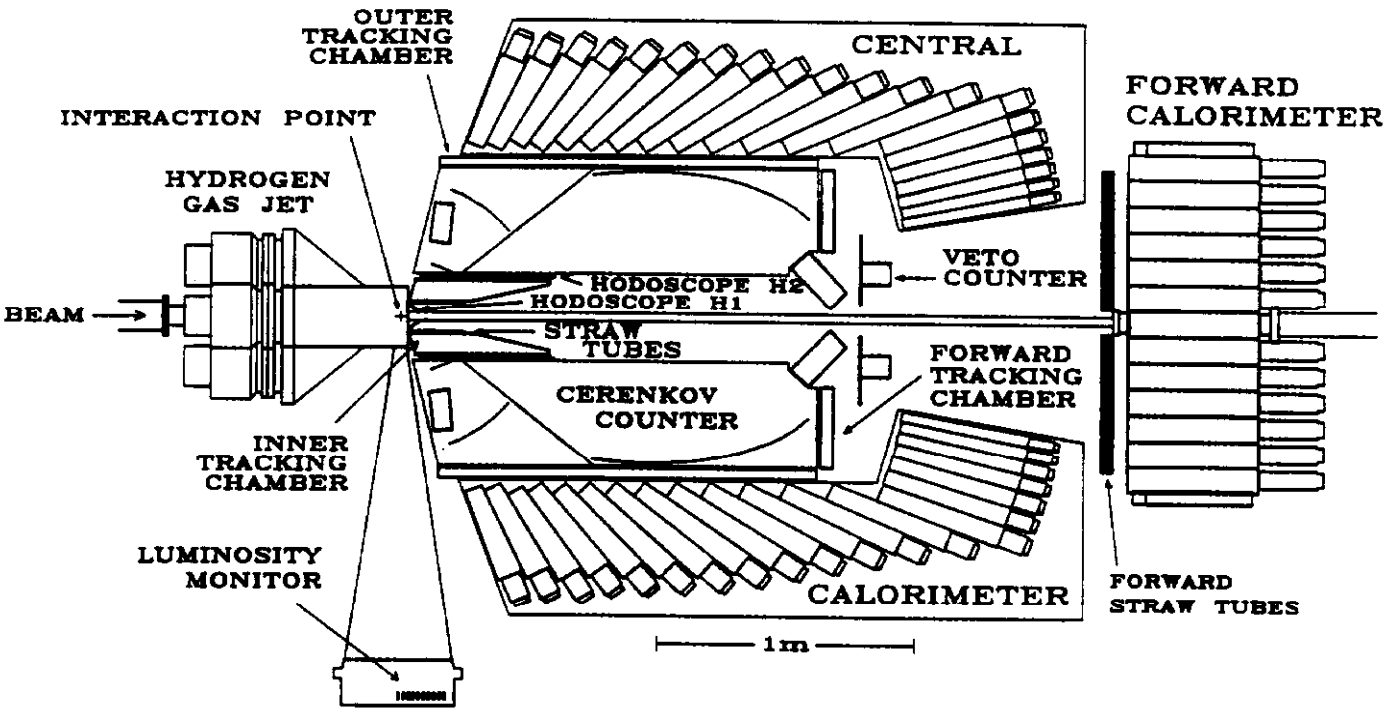

Figure 10. The E760 detector.

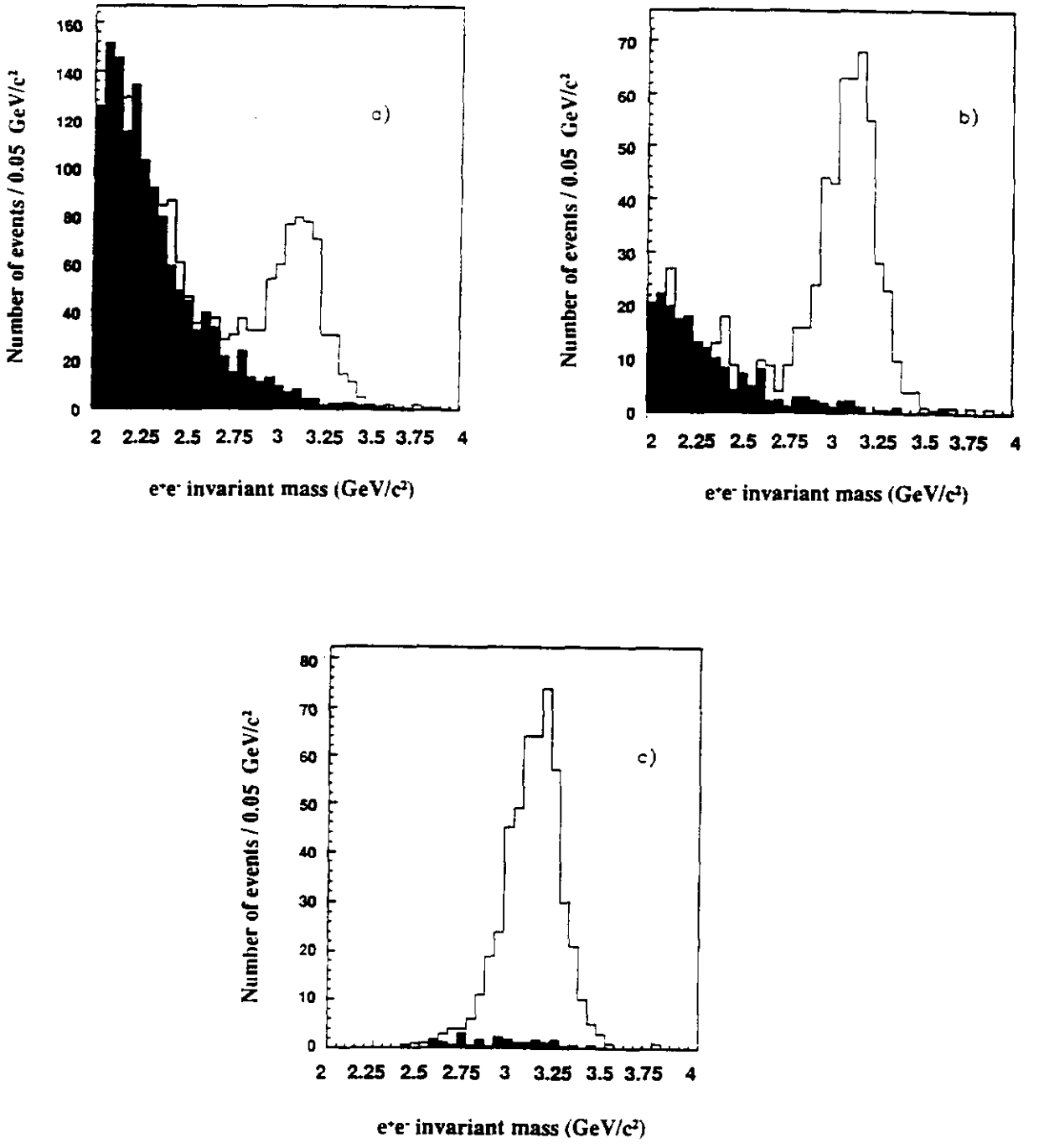

Figure 11. Invariant mass distribution of electron-positron pair at the $^3P_1$ energy for events passing a) the preliminary selection; b) the inclusive selection where the electron and positron must both satisfy an electron quality index ; c) the exclusive selection where the event must satisfy a kinematical fit. The shaded area is the invariant mass distribution accumulated off-resonance for an equivalent luminosity (background).

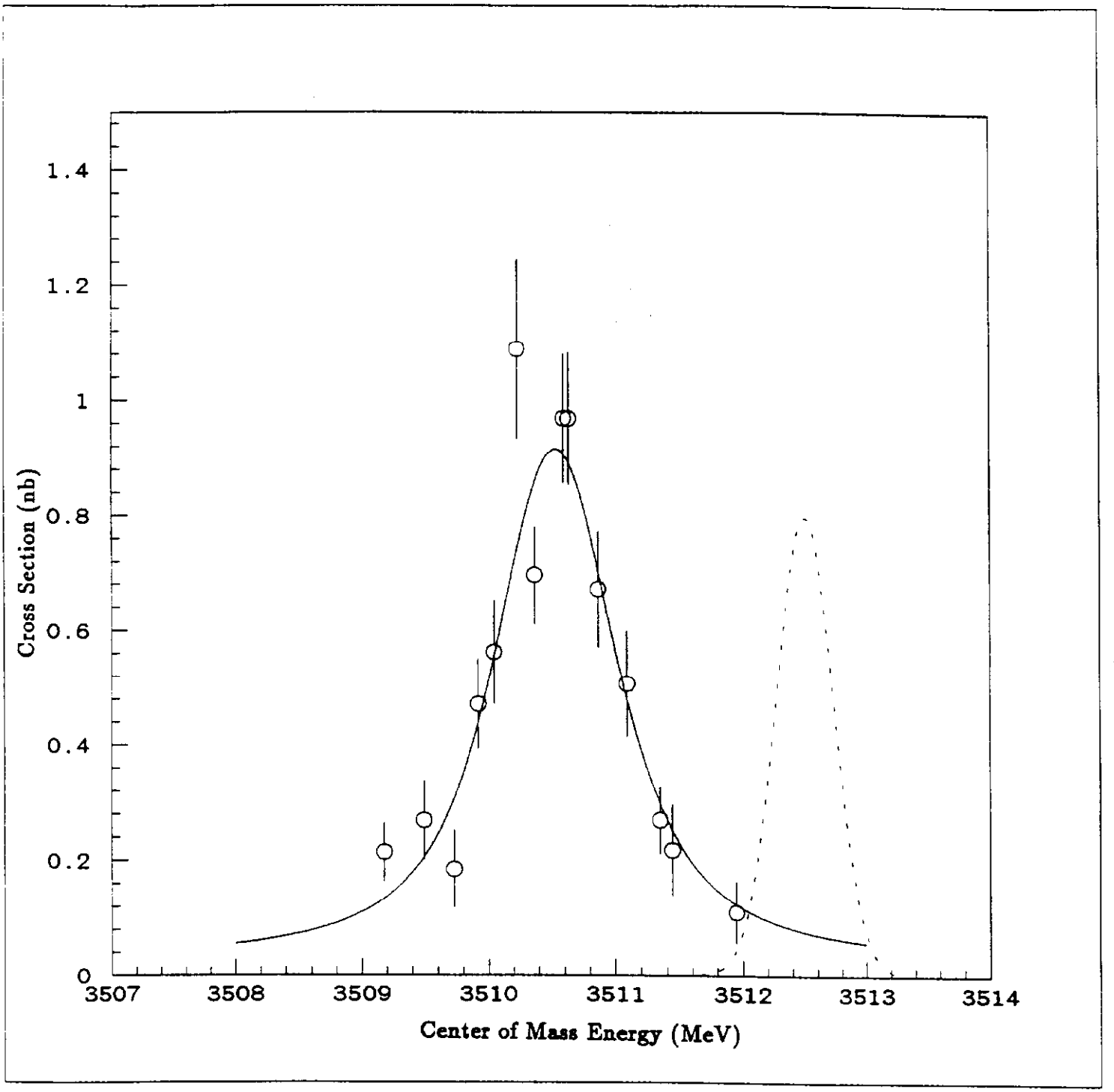

Figure 12. Excitation curve for the $^3P_1$ resonance . The dashed line is a typical beam energy profile at this energy.

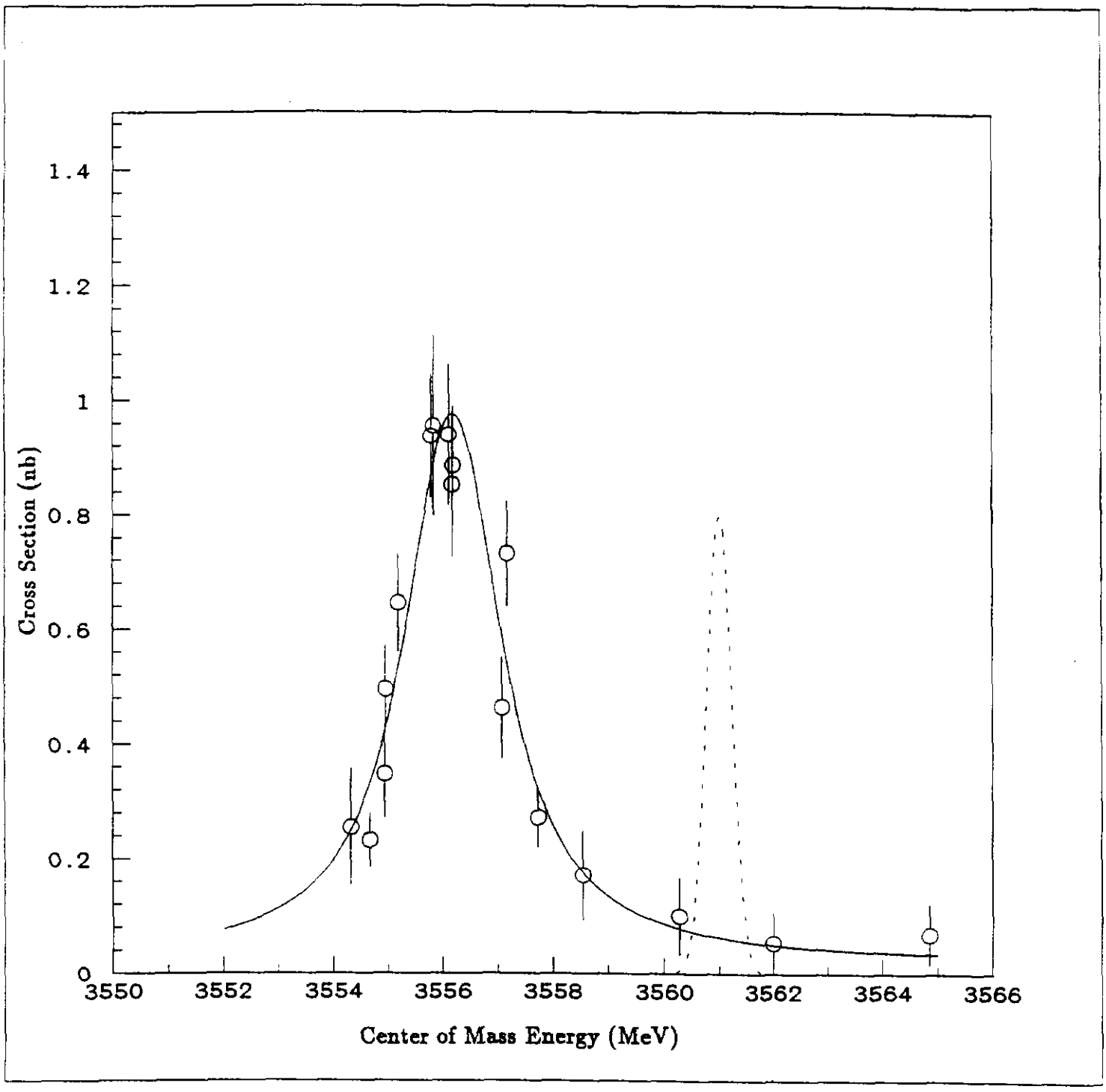

Figure 13. Excitation curve for the $^3P_2$ resonance. The dashed line is a typical beam energy profile at this energy.

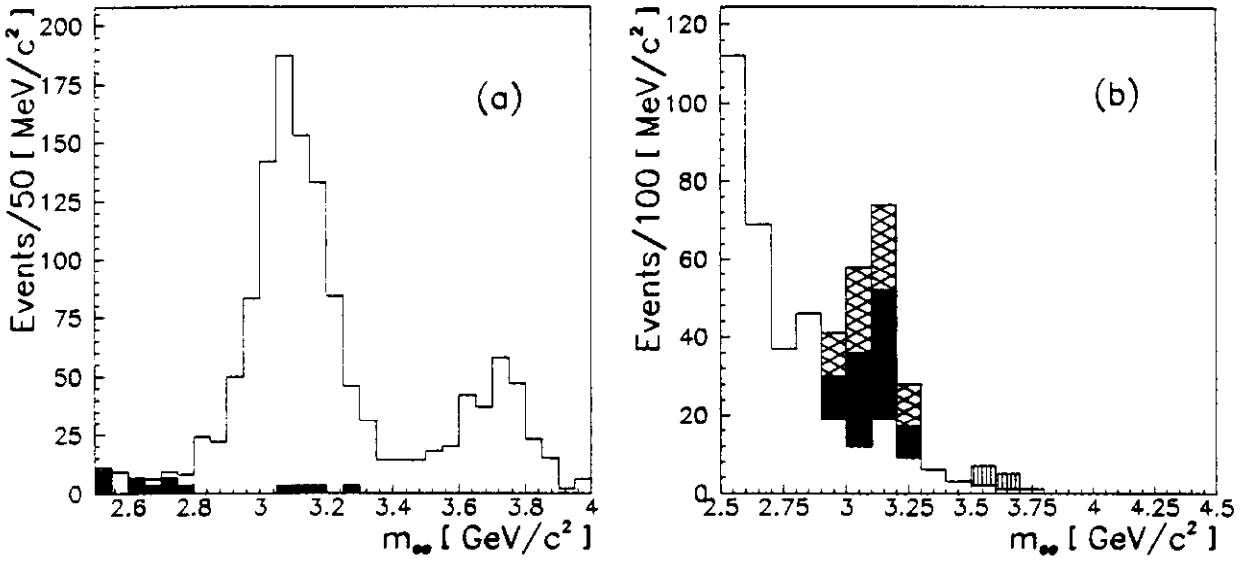

Figure 14. Invariant mass distribution of electron-positron pair taken at a) the Ψ' resonance (~1 pb^{-1} of integrated luminosity) and b) near the center-of-gravity of the ^3P states (~16 pb^{-1} of integrated luminosity). The shading in b) is described in the text.

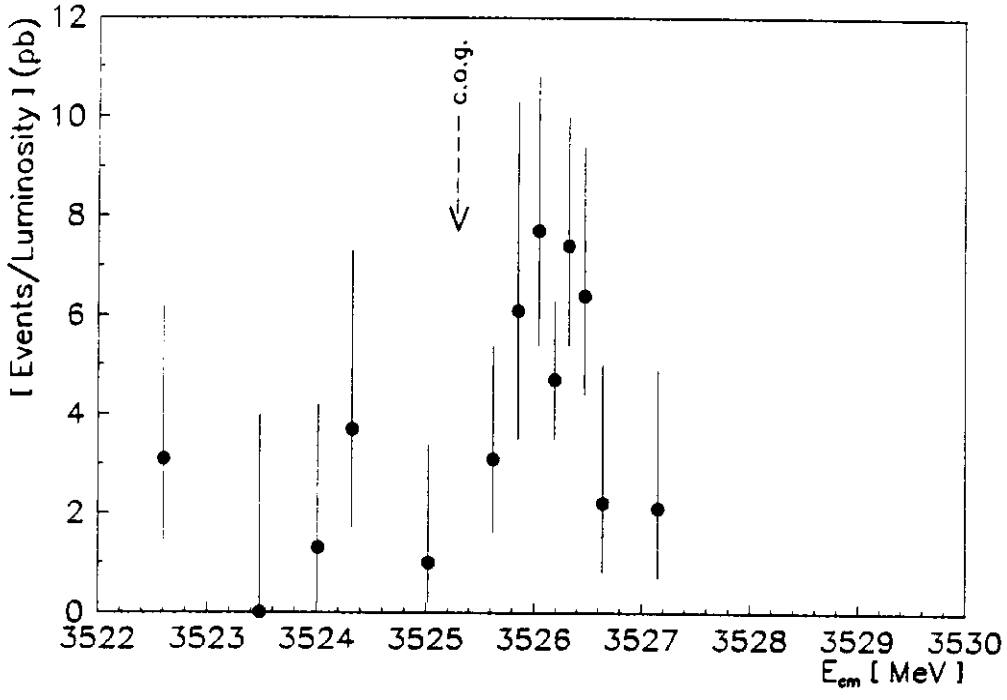

Figure 15. Cross section versus center-of-mass energy near the center-of-gravity.

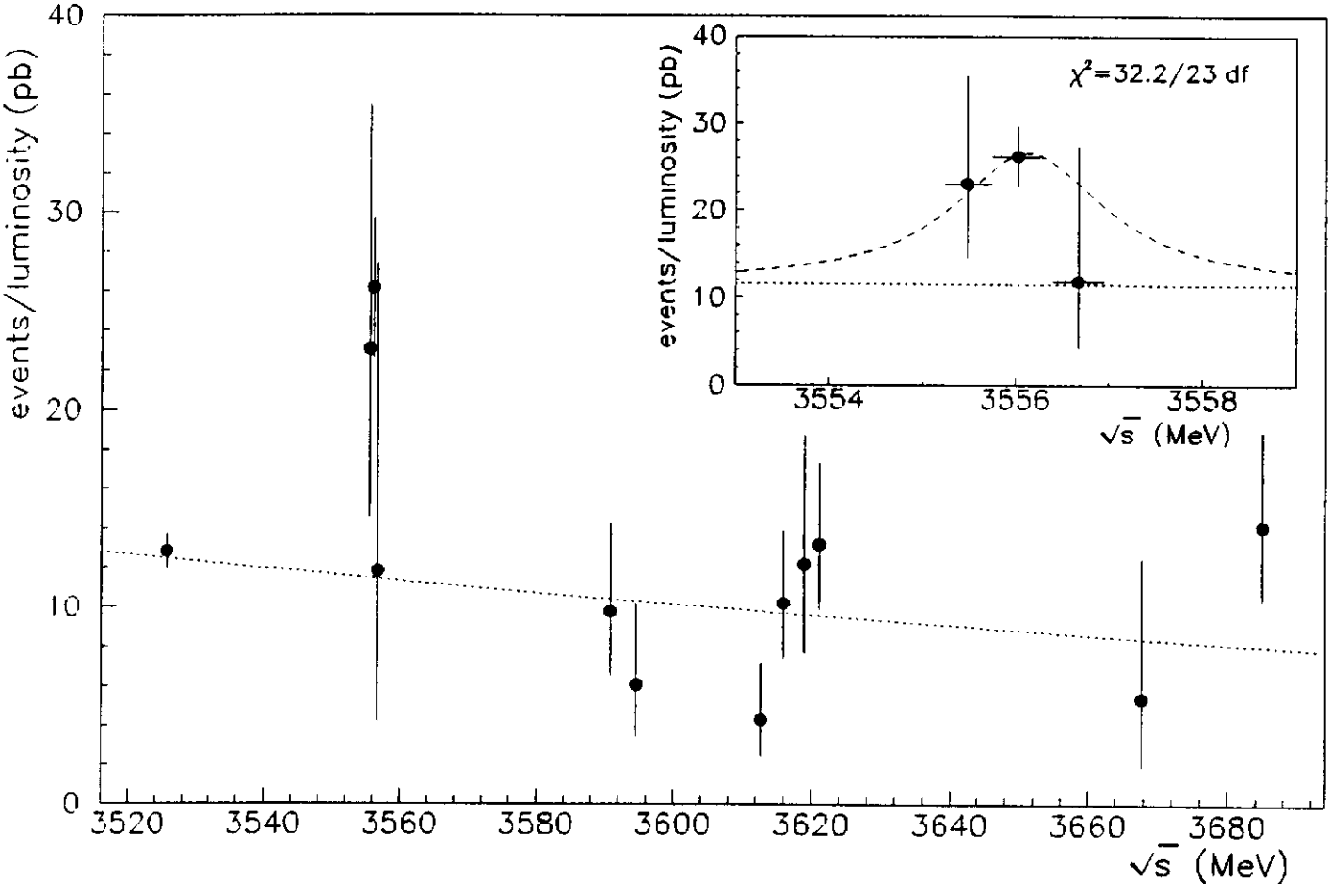

Figure 16. Two gamma cross section in the region of the $^3P_2$ state.

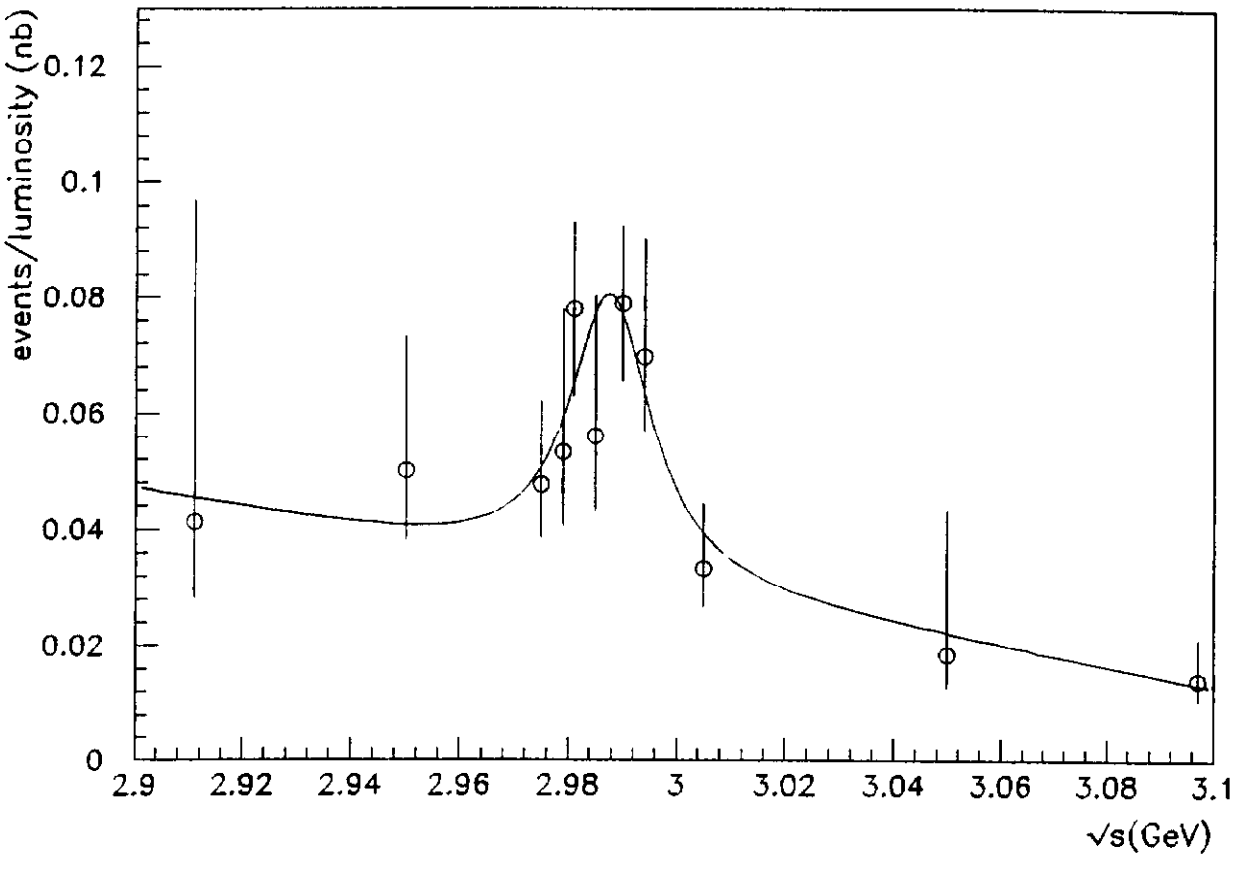

Figure 17. Two gamma cross section in the region of the $^1S_0$ state.